HHS Public Access

Author manuscript

Cell Rep. Author manuscript; available in PMC 2023 May 25.

Published in final edited form as:

Cell Rep. 2023 March 28; 42(3): 112237. doi:10.1016/j.celrep.2023.112237.

Jarid2 promotes temporal progression of retinal progenitors via repression of *Foxp1*

Jianmin Zhang[1,3], **Jacqueline M. Roberts**[1,3], **Fei Chang**[1,2,3], **Joon Schwakopf**[1], **Monica L. Vetter**[1,4,*]

[1]Department of Neurobiology, University of Utah Spencer Fox Eccles School of Medicine, Salt Lake City, UT 84112, USA

[2]Interdepartmental Program in Neuroscience, University of Utah Spencer Fox Eccles School of Medicine, Salt Lake City, UT 84112, USA

[3]These authors contributed equally

[4]Lead contact

SUMMARY

Transitions in competence underlie the ability of CNS progenitors to generate a diversity of neurons and glia. Retinal progenitor cells in mouse generate early-born cell types embryonically and late-born cell types largely postnatally. We find that the transition from early to late progenitor competence is regulated by Jarid2. Loss of *Jarid2* results in extended production of early cell types and extended expression of early progenitor genes. Jarid2 can regulate histone modifications, and we find reduction of repressive mark H3K27me3 on a subset of early progenitor genes with loss of *Jarid2*, most notably *Foxp1*. We show that *Foxp1* regulates the competence to generate early-born retinal cell types, promotes early and represses late progenitor gene expression, and is required for extending early retinal cell production after loss of *Jarid2*. We conclude that *Jarid2* facilitates progression of retinal progenitor temporal identity by repressing *Foxp1*, which is a primary regulator of early temporal patterning.

In brief

Temporal patterning of neural progenitors is essential to generate neuronal diversity. Zhang et al. find that Jarid2 facilitates retinal progenitor temporal identity transition via H3K27me3 deposition and repression of early genes, most notably *Foxp1*. They find that *Foxp1* is an effector of *Jarid2* in regulating timing of retinal neurogenesis.

*Correspondence: monica.vetter@neuro.utah.edu.

AUTHOR CONTRIBUTIONS

Conceptualization, M.L.V.; methodology, J.Z., J.M.R., F.C., and M.L.V.; image analysis, J.Z., F.C., and J.S.; bioinformatical analysis, J.M.R.; manuscript preparation and writing: J.Z., J.M.R., F.C., and M.L.V.; funding acquisition, M.L.V.

DECLARATION OF INTERESTS

J.Z., J.M.B., F.C., and M.L.V. are co-inventors on a provisional patent (US Provisional Patent Serial No. 63/439,941) that incorporates technology described in this article.

SUPPLEMENTAL INFORMATION

Supplemental information can be found online at https://doi.org/10.1016/j.celrep.2023.112237.

Graphical Abstract

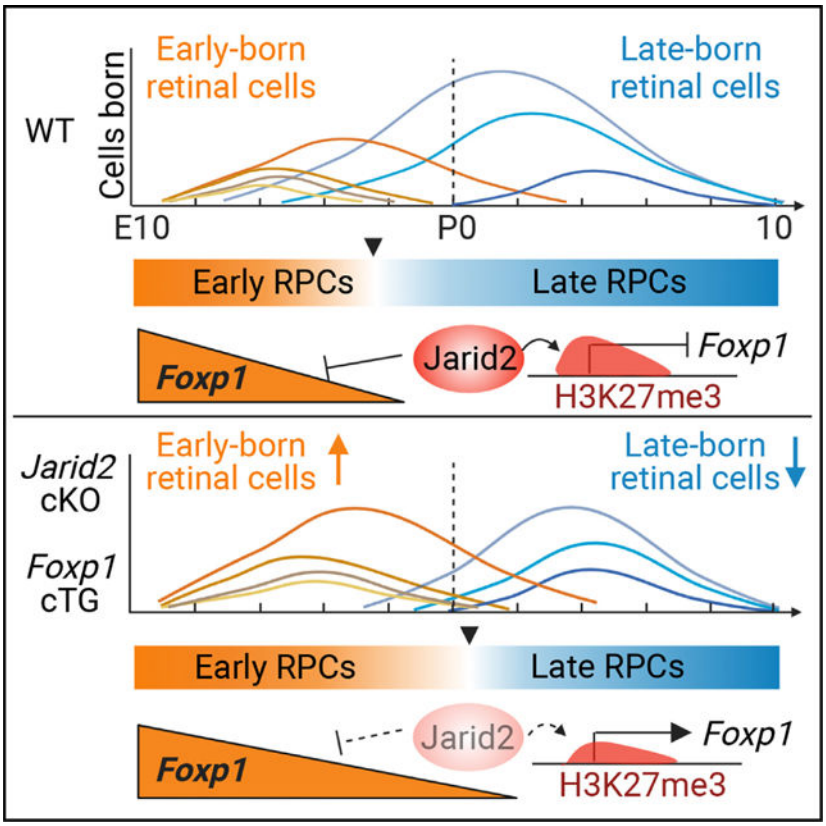

INTRODUCTION

Temporal patterning of progenitors is critical for generating a diversity of cell types during development of the nervous system, driving the differentiation of neurons and glia in specific proportions in a defined sequence.[1,2] Changes in neural progenitor competence govern the ability of progenitors to differentiate into diverse neuronal and glial cell types.[3,4] A major challenge is determining how regulation of temporal competence in the vertebrate central nervous system (CNS) is coordinated by transcriptional programs and changes in chromatin accessibility.[1,2,5–7]

This problem is well defined in the developing retina, since lineage analysis has shown that multipotent retinal progenitor cells (RPCs) progress through temporally regulated competence states during which they generate distinct cell types in a defined sequence that is conserved across species.[5,8] In the mouse, early-born cell types (retinal ganglion cells [RGCs], cone photoreceptors, horizontal cells, some amacrine cells) are generated embryonically, while late-born cell types (most rod photoreceptors, remaining amacrine cells, bipolar cells, Müller glia) are generated postnatally, with precise regulation of cell fate specification.[7] Cell-intrinsic processes primarily regulate the timing of cell genesis, with late progenitors restricted from generating earlier cell types.[8–10] Recent single-cell analysis of mouse and human retinal development has revealed a distinct shift in gene expression

and chromatin accessibility from early- to late-stage RPCs, consistent with a change in competence to generate early- versus late-born retinal cell types.[11–13] Multiple temporal identity factors and regulators have been shown to regulate RPC competence and timing of retinal cell production, including those with similarity to temporal identity factors first identified in *Drosophila* such as Ikaros family (Ikzf1 and Ikzf4) and Casz1, as well as other transcription factors such as FoxN4, Pou2f1/Pou2f2, Lhx2, and NFI factors, along with microRNA regulation through Dicer.[11,13–25] However, whether additional factors contribute to, and the molecular mechanisms regulating, progressive changes in RPC competence are still unclear.

Histone modifications contribute to changes in the ability of CNS progenitors to generate diverse cell types,[3,6,17,26,27] and also play a role in retinal development.[28] A key repressive histone modification, methylation of H3 at lysine 27 (H3K27me3) is dynamically regulated on progenitor and differentiation genes during mouse and human retinal development.[29] H3K27 methylation is catalyzed by polycomb repressive complex 2 (PRC2), which is composed of obligate core components and an array of accessory proteins.[30] PRC2 plays important developmental roles in multiple embryonic lineages including the developing nervous system.[27,31,32] In retinal progenitors, loss of core components, Ezh2 or Eed, results in widespread derepression of genes not normally expressed in retinal lineages, accelerated differentiation of late-born cell types, as well as premature cell-cycle exit resulting in progenitor depletion.[33–35] These findings suggest that PRC2-mediated gene repression maintains retinal lineage integrity and regulates progenitor differentiation.

Jarid2 (Jumonji, AT-rich interactive domain 2) is best characterized as a component of PRC2.2, one of two alternate subcomplexes that methylate H3K27,[36–40] and Jarid2 can also associate with complexes that methylate H3K9.[41,42] *Jarid2* is required for embryonic development, including brain development, as well as transition between pluripotent and differentiated states of embryonic stem cells (ESCs), although its *in vivo* function, particularly in CNS development, is not fully defined.[39,43–46] In humans, the JARID2 gene is associated with autism spectrum disorder, schizophrenia, and neurodevelopmental delay.[47–51] Since *Jarid2* has been implicated in CNS development, and plays a role in regulating histone modification and gene repression, we sought to further investigate its function.

Here, we show that *Jarid2* is important for temporal patterning of progenitors, facilitating the progression from early to late RPCs. Conditional loss of *Jarid2* resulted in a delayed transition from early to late RPC gene expression, and extended production of early-born retinal cell types. We also observed selective loss of H3K27me3 and derepression for a subset of genes expressed in early RPCs, most notably the transcription factor *Foxp1*. Through gain- and loss-of-function analysis, we show that *Foxp1* promotes the production of early retinal cell types, and functions as a key effector in extending early retinal cell production after loss of *Jarid2*. We conclude that *Jarid2* promotes repression of *Foxp1* to facilitate the progression from early to late RPC competence.

RESULTS

Loss of Jarid2 affects retinal neurogenesis

We first sought to examine the expression of *Jarid2*, so we performed *in situ* hybridization on sections of E14.5 and P0 mouse retina and found that *Jarid2* is expressed in retinal progenitors in the neuroblastic layer and differentiating cells in the ganglion cell layer (GCL) (Figures S1A–S1D). To address its function, we conditionally inactivated *Jarid2* in retinal progenitors prior to onset of neurogenesis using either *Six3-Cre* (*Six3-Cre Jarid2* cKO)[52] or *Rax-CreER*^{T2}, a tamoxifen-inducible Cre (*Rax-Cre Jarid2* cKO)[53] (Figure S1E). Tamoxifen interferes with birth, so *Rax-Cre Jarid2* cKO pups were collected embryonically, while *Six3-Cre Jarid2* cKO was used for postnatal analysis. We confirmed reduction of full-length *Jarid2* mRNA from *Six3-Cre Jarid2* cKO retina at P0 by RT-PCR (Figure S1F), and by sequencing the knockout product confirmed loss of exon 3, which results in a frameshift and premature stop. We also confirmed reduced protein expression by western blot (Figure S1G).

During mouse retina development, RGCs, horizontal cells, cone photoreceptors, and some amacrine cells are born during the embryonic period, so we asked whether the generation of these early-born cell populations is impacted by loss of *Jarid2*. We generated *Rax-Cre Jarid2* cKO by administering tamoxifen at onset of retinal neurogenesis at E10.5,[53] and collected embryos at E18.5 after early cell genesis is largely complete. In *Rax-Cre Jarid2* cKO retina we observed increased Brn3a+ RGCs in the GCL (Figures 1A, 1B, and 1I). There was also an increase in the number of Rxrγ+ cone photoreceptors (Figures 1C, 1D, and 1J) and increased Calbindin+ horizontal cells in outer retina (Figures 1E, 1F, and 1K). Calbindin also labels a subset of amacrine cells and RGCs, and we found increased Calbindin+ cells in the inner retina (Figures 1E, 1F, and 1L). Consistent with this, there were increased AP2α+ amacrine cells (Figures 1G, 1H, and 1M). We confirmed increased Brn3+ RGCs in *Six3-Cre Jarid2* cKO at P0 (Figures S2A, S2B, and S2G). In *Six3-Cre Jarid2* cKO there were also increased Calbindin+ amacrine cells (Figures S2C, S2D, and S2H) and increased Rxrγ+ cone photoreceptors (Figures S2E, S2F, and S2I). We found no difference in pH3-labeled mitotic cells at E18.5 in *Rax-Cre Jarid2* cKO retina ($p = 0.18$, Table S6), suggesting that proliferation did not contribute to the shift in early cell number. We did observe an increase in cleaved caspase-3-labeled apoptotic cells at P0 in *Six3-Cre Jarid2* cKO retina ($p < 0.05$, Table S6), but still found that the increased early-born cells persisted, with increased Brn3a+ RGCs, AP2α+ amacrine cells, and Rxrγ+ cone photoreceptors evident in the *Six3-Cre Jarid2* cKO retina at P14 (Figures S2S–S2AA). Thus, loss of *Jarid2* results in an overall increase in early-born retinal cell populations.

One possible explanation for this phenotype is increased production of these cells during their normal developmental window. To address this, we performed analysis of *Six3-Cre Jarid2* cKO at E16.5 when early cell genesis is still ongoing. At that time point, we detected no change in the number of Brn3+ RGCs (Figures S2J, S2K, and S2P), Otx2+ photoreceptor precursors (Figures S2L, S2M, and S2Q), or Rxrγ+ cone photoreceptors (Figures S2N, S2O, and S2R). Thus, we conclude that there is not an increased production of these cell populations during the initial period of early cell genesis.

We hypothesized that the increased early-born retinal cells may potentially affect the generation of rod photoreceptors, bipolar cells, and Müller glia, which are largely born after birth. We found a reduced number of photoreceptors labeled for Recoverin in the central retina at P0 in *Six3-Cre Jarid2* cKO (Figures 1N, 1O, and 1T). Retinal neuron differentiation follows a central to peripheral gradient, and at the periphery we found that the leading edge of Recoverin labeling was more central in the cKO, suggesting delayed photoreceptor differentiation (Figures 1N′ and 1O′). At P14 the number of Vsx2+ bipolar cells was reduced in *Six3-Cre Jarid2* cKO (Figures 1P, 1Q, and 1U), but there was no apparent change in Lhx2+ Müller glia (Figures 1R, 1S, and 1V). Together, we conclude that, with loss of *Jarid2*, there is enhanced production of early-born retinal neurons during the late embryonic period, and consequently reduced production of later born retinal neurons, suggesting a delayed shift from early to late retinal cell generation.

Loss of Jarid2 results in extended production of early-born retinal neurons

To directly assess whether there is increased production of early retinal cell types during the late embryonic period, we labeled mitotic cells by administering EdU at E16.5 and E17.5, followed by EdU detection and immunostaining for differentiated cell markers at E18.5 (Figure S3A). Compared with controls, *Rax-Cre Jarid2* KO retinas showed a significant increase in EdU+Brn3a+ RGCs (Figures S3B, S3C, and S3H). Similarly, we detected an increase in EdU+AP2α+ amacrine cells (Figures S3D, S3E, and S3I) and in EdU+Rxrγ+ cone photoreceptors (Figures S3F, S3G, and S3J). These findings indicate that, with loss of *Jarid2*, there is increased production of multiple early retinal cell types during the late embryonic period, from E16.5 to birth.

Inactivation of *Jarid2* may lead to an increased production of early-born cell types toward the end of their normal window of production, or may extend the window. To distinguish between these possibilities, we administered EdU to control and *Six3-Cre Jarid2* cKO animals at E18.5, after all early retinal cell types are normally generated,[54] then performed analysis at P0 (Figure 2G). We first asked whether there is a change in cell-cycle exit by combining EdU detection with immunostaining for mitotic marker PCNA. We found that the percent EdU+PCNA−/EdU+ cells was increased, indicating that loss of *Jarid2* promotes enhanced cell-cycle exit of progenitors (Figure 2H). When we immunostained for markers of early retinal cell types, control retinas showed no EdU+Brn3a+ RGCs, consistent with RGC genesis being complete. In contrast, EdU+Brn3a+ RGCs were evident in *Six3-Cre Jarid2* cKO retinas, although this did not reach significance due to low number and variability ($p = 0.08$; Figures 2A, 2B, and 2I). Similarly, control retinas showed no EdU+Oc2+ horizontal cells nor EdU+ Rxrγ+ cone photoreceptors, while these were significantly increased in *Six3-Cre Jarid2* cKO retinas (Figures 2C–2F, 2J, and 2K). Thus, loss of *Jarid2* promotes RPC differentiation with extended production of multiple early-born cell types beyond their normal developmental window.

Loss of Jarid2 results in increased early-stage RPC gene expression

Prior single-cell RNA sequencing (scRNA-seq) analysis of gene expression across the course of retinal neurogenesis (E11–P14) showed a shift from early to late RPC gene expression signatures between E16.5 and E18.5.[11] We hypothesized that this transition may

be delayed with loss of *Jarid2*. To determine whether RPC gene expression is altered, we performed scRNA-seq on cells isolated from whole retinas of *Rax-Cre Jarid2* cKO and littermate controls at E18.5, and performed the experiment twice to obtain two biological replicates for each sample. We saw a clear overlap between the two batches and genotypes (Figures S4C and S4D), and we identified retinal cell types using established markers (Figures 3A, S4A, and S4B).[11] We performed dimensional reduction using spliced transcript counts to narrow the window of gene expression to only mature transcripts. Interestingly, we observed that *Jarid2* cKO and control cells were distinguishable in the primary RPC population, arguing that gene expression in this cell population is changed with loss of *Jarid2* (Figure 3B).

To understand the molecular basis for extended generation of early retinal cell types, we focused on primary RPCs and found 125 upregulated and 105 downregulated genes in *Jarid2* cKO RPCs compared with control RPCs (Figure 3D, Table S1). We sought to compare these to genes previously found to be enriched in early versus late RPCs, so we reanalyzed published scRNA-seq data to visualize expression of select RPC genes from E11 to P5[11] (Figure S5). We found that *Jarid2* cKO primary RPCs showed significantly increased expression of multiple early-stage RPC genes, including *Foxp1*, *Sfrp2*, *Itm2a*, *Nr2f1*, *Col9a1*, and *Fgf15*, while multiple late-stage RPC genes, including *Ndufa4l2*, *Car2*, *Gas1*, *Cox4l2*, *Isl1*, and *Ascl1*, were decreased (Figures 3C and 3D).

To investigate the possibility of a delayed shift to late-stage RPCs in the absence of *Jarid2*, we directly compared our findings to gene expression data from E11 to P5 RPCs.[11] Using Monocle,[55] we identified gene sets, or modules, from this dataset that vary across developing RPCs (Table S2). We compared aggregated module gene expression of RPCs at each time point to that of *Jarid2* cKO and control RPCs (Figure 3E). This analysis found that *Jarid2* cKO RPCs from E18.5 retinas showed greater similarity in module gene expression to early RPCs (E16.5 and earlier), while *Jarid2* control RPCs were more similar to late RPCs (E18.5 and later). Altogether, these findings suggest that loss of *Jarid2* results in a delay in the transition from early to late-stage RPCs.

Jarid2 regulates H3K27me3 deposition on genes expressed in early RPCs

Since Jarid2 can regulate PRC2 activity and recruitment to target genes,[36,56] we hypothesized that the observed transcriptional differences in the *Jarid2* cKO could be attributed to changes in H3K27me3-mediated gene repression. To test this, we performed CUT&RUN chromatin profiling to define the distribution of H3K27me3 modification in control and *Rax-Cre Jarid2* cKO retinas at E18.5. Altogether, we generated 8 samples each from *Jarid2* cKO and control animals, in two separate batches. We identified 19,034 H3K27me3-enriched peaks in the control and *Jarid2* cKO samples, with 840 significantly increased and 744 significantly decreased in *Jarid2* cKO retinas (Figure 4A; Table S3). To reveal cohorts of genes that may be important for the change in temporal patterning of RPCs in *Jarid2* cKO, we identified genes associated with differential H3K27me3 peaks that are also differentially expressed in *Rax-Cre Jarid2* cKO RPCs (Figure 4B). Since Jarid2 is reported to promote transcriptional repression, we focused on those that lose H3K27me3 repression and have higher RNA expression in the *Jarid2* cKO RPCs. Among these, the early

RPC gene *Foxp1* was notable due its increased expression in *Jarid2* cKO RPCs combined with decreased H3K27me3, with at least seven significantly decreased peaks in or near the *Foxp1* locus (Figures 4B and 4C).

To identify the changes in H3K27me3 distribution during early versus late retinal development, we performed CUT&RUN analysis on E14.5 retina during peak early cell production, and on P0 retina, when early cell genesis is complete and late cell production has begun. We observed sparse H3K27me3 labeling of the *Foxp1* locus at E14.5, with a substantial increase by P0 (Figure 4D). An inspection of prior H3K27me3 ChIP data across retinal development[29] showed that similar regions within the *Foxp1* locus progressively acquire H3K27me3 during normal retinal development, from E17.5 to P3 (Figures S6A and S6B). These data suggest that Jarid2 facilitates *Foxp1* repression via H3K27me3 deposition during the transition from early to late retinal cell production. Similarly, several previously identified Jarid2 target genes (*Pcdh7*, *Fign*, *Efna5*, and *Reln*) show reduced H3K27me3 and increased expression in *Jarid2* cKO RPCs (Figure 4B). These genes are also expressed in early RPCs (Figure S5) and acquire H3K27me3 from early (E14.5) to late (P0) stages (Figure S6),[45,56] although the effect on *Foxp1* was the most robust. Altogether, the intersection of H3K27me3 profiling combined with scRNA-seq suggests that *Jarid2* promotes the repression of a subset of genes expressed in early RPCs during the transition from early to late RPC states.

Foxp1 regulates the generation of early-born retinal cell types

To better understand genes that may mediate *Jarid2* function in RPC competence transitions, we focused our attention on *Foxp1*, since it encodes a transcription factor, and is thus most likely to mediate changes in temporal competence of progenitors. In addition, *Foxp1* has been shown to regulate the window for early neurogenesis during cortical development.[57] In the developing retina, *Foxp1* was reported as an early RPC gene and shown to decline in expression by E17.5 (Figure S5).[11,13,58] To better define *Foxp1* temporal expression in the developing mouse retina, we used antibody detection and found that it is expressed in RPCs in the neuroblastic layer at E12.5 and E14.5, with declining expression at E16.5, and virtually no detectable expression in RPCs at P0 (Figure 5A). We saw strong expression of *Foxp1* in a subset of RGCs as reported previously[58,59] (Figure 5A). Thus, *Foxp1* is downregulated in RPCs during the transition from early to late retinal neurogenesis, consistent with the increased H3K27me3-mediated repression we detected at the *Foxp1* locus (Figure 4D).

To determine the function of *Foxp1* in early RPCs, we conditionally abolished *Foxp1* expression by crossing *Six3-Cre* mice with *Foxp1*-floxed mice (*Foxp1* cKO),[60] and used littermates lacking Cre as controls. The efficiency of *Foxp1* cKO in the retina was confirmed by *Foxp1* immunostaining at E14.5 (Figures 5B and 5C). To test if the generation of early-born cell types was affected in *Foxp1* cKO, we performed immunostaining at P0 for early-born retinal cell type markers. All cell types were present, as reported previously for *Dkk3-Cre*-mediated *Foxp1* cKO,[58] so we quantified to detect potential shifts in their proportions. We observed a thinning of the GCL and a significant reduction in Brn3a+ RGCs (Figures 5D, 5E, and 5J). We also found a significant reduction in Calbindin+

horizontal cells in the outer retina (Figures 5F, 5G, and 5K), and a significant reduction in Rxrγ+ cone photoreceptors (Figures 5H, 5I, and 5L). Together this suggests that *Foxp1* promotes early-born cell generation. To determine whether the loss of *Foxp1* alters the transcriptional profile of RPCs, we performed bulk RNA-seq on E16.5 *Foxp1* cKO and littermate control retinas. Several early RPC genes, including *Itm2a*, *Ndufa4*, and *Col9a1*, were downregulated, while a group of late RPC genes, such as *Casz1*, *Nfib*, and *Sox9*, were upregulated, indicating premature expression of late RPC genes in *Foxp1* cKO (Figure 5M; Table S4).

We have shown that *Jarid2* cKO results in elevated *Foxp1* expression at the late embryonic stage, and that loss of Foxp1 reduces early-born cell generation, which is the opposite of the *Jarid2* cKO phenotype. Based on these observations, we hypothesized that loss of *Jarid2*-mediated repression of *Foxp1* could be a major factor in the delayed transition to late progenitor competence and extended production of early cell types. To test this, we generated *Foxp1*:*Jarid2* double cKO animals using *Six3-Cre*. We confirmed that *Six3-Cre Jarid2* cKO mice showed increased Brn3a+ RGCs at P0 (Figures 5N, 5O, and 5W). In contrast, *Foxp1*:*Jarid2* double cKO mice showed no significant change in Brn3a+ RGCs compared with littermate controls lacking Cre (Figures 5N, 5P, and 5W). Similarly, the increase in Calbindin+ horizontal cells and Rxrγ+ cone photoreceptors seen in *Jarid2* cKO retinas were also reversed in *Foxp1*:*Jarid2* double cKO mice (Figures 5Q–5V, 5X, and 5Y). Thus, elevated *Foxp1* is required for increased early-born cell production after loss of *Jarid2*.

Ectopic Foxp1 expression in RPCs affects retinal cell genesis

Since *Foxp1* expression normally declines and is absent in RPCs by P0, we asked whether sustained *Foxp1* expression is sufficient for the generation of early-born neurons. We conditionally elevated *Foxp1* in RPCs by crossing *Six3-Cre* mice with conditional *Foxp1* transgenic mice expressing *Foxp1* under the CAG promoter (*Foxp1* cTG).[61] We confirmed by immunostaining that Foxp1 expression was increased in retinal progenitors of Six3-Cre *Foxp1*$^{tg/+}$ mice, with mosaic levels of expression in radial columns (Figures 6A, 6B, S7A, and S7B). We then assessed effects on the generation of early cell types and found that by P0, overexpression of *Foxp1* led to an increase in Brn3a+ RGCs in the GCL similar to the *Jarid2* cKO phenotype (Figures 6C, 6D, and 6K). We also observed a significant increase in other early-born cell types, including Onecut2+ horizontal cells (Figures 6E, 6F, and 6L), and Rxrγ+ cone photoreceptors (Figures 6G, 6H, and 6M). We observed more Brn3a+ RGCs in regions with higher *Foxp1* levels in *Six3-Cre Foxp1*$^{tg/+}$ mice (Figures S7C–S7E), suggesting that RGC generation may be *Foxp1* dosage dependent. To test this, we analyzed *Foxp1* cTG mice with two copies of the *Foxp1* transgene and found that Brn3a+ RGCs were dramatically increased in (Figures 6I and 6J).

We then asked whether there was a corresponding effect on late-born cell generation by examining *Foxp1* cTG retina at P10. We found a reduction in late-born retinal cells including Vsx2+ bipolar cells (Figures 6N, 6O, and 6T) and Rhodopsin+ rod photoreceptors (Figures 6P, 6Q, and 6U). This is consistent with a prior study showing increased cones and reduced rods following *Foxp1* overexpression.[58] We also observed disruption of the outer limiting membrane with abnormal Rhodopsin+ cells in the subretinal space (Figures

6P and 6Q) in *Foxp1* cTG, although the severity of such aberrant rosette-like structures was variable across sections and animals (Figures S7F–S7H). We found that Lhx2+ and Cralbp+ Müller glia were reduced in the inner nuclear layer (Figures 6R, 6S, and 6V), and some were mislocated to the outer plexiform layer and outer nuclear layer (Figure 6V′). Thus, late-born cell generation is reduced and Müller glia development impacted by misexpression of *Foxp1*.

To determine if the increased generation of early-born retinal cells was due to an extended window of production, we administered EdU to *Foxp1* cTG mice at E18.5 and performed immunostaining for Brn3a+ RGCs at P0. Control retinas showed no Brn3a+ RGCs colabeled with EdU, in contrast to *Foxp1* cTG retinas (Figures 6W–6Z), indicating an extended window of RGC genesis. As in *Jarid2* cKO, this extended window was coupled with enhanced exit of RPCs, as we found that the percentage of EdU+PCNA−/EdU+ cells was increased (Figure 6AA). Taken together these results suggest that *Foxp1* promotes the generation of early-born retinal cells at the expense of late-born cell generation by extending the window of early cell genesis.

Sustaining Foxp1 in RPCs maintains early RPC transcription pattern

To assess if *Foxp1* overexpression in RPCs changes the gene expression pattern of RPCs, we performed scRNA-seq on P0 *Foxp1* cTG and control littermate retinas (Figure 7A). We observed a dramatic difference in the UMAP embedding of RPCs between *Foxp1* cTG and control retinas (Figure 7B). Focusing our analysis on RPCs, we identified 575 differentially expressed genes in the *Foxp1* cTG retinas. We noted upregulation of early RPC genes, including *Sfrp2*, *Col9a1*, *Fgf15*, and *Itm2a*, and downregulation of late RPC genes *Ndufa4l2*, *Car2*, *Casz1*, and *Nfib*, suggesting that an early RPC transcriptional pattern is artificially maintained in *Foxp1* cTG RPCs (Figures 7C and 7D).

As the gene expression pattern in *Foxp1* cTG RPCs is reminiscent of that in *Jarid2* cKO RPCs we compared the genes that were significantly differentially expressed in these two datasets. We found that, of the 230 genes differentially expressed in *Jarid2* cKO and 575 in *Foxp1* cTG RPCs, 96 were differentially expressed in both conditions. Among these, 96 genes are upregulated early RPC genes (*Fgf15*, *Sfrp2*, *Itm2a*, *Pcdh7*, *Ppl35*, *Rpl27a*, and *Col9a1*) and downregulated late RPC genes (*Car2*, *Gas1*, and *Ndufa4l2)* (Figure 7E). The large overlap between these two datasets suggests that Foxp1 and Jarid2 may regulate similar biological processes.

We took an unbiased approach to define the biological processes altered in *Jarid2* cKO and *Foxp1* cTG RPCs. Significantly altered MSigDB mouse hallmark gene sets were identified from each dataset through preranked gene set enrichment analysis (Figure 7F).[62] We found that two gene sets were significantly depleted in both *Jarid2* cKO and *Foxp1* cTG RPCs: Myc targets V1 and hypoxia. Several additional gene sets were significantly reduced in *Foxp1* cTG, with *Jarid2* cKO data trending in the same direction: E2F targets, G2M checkpoint, P53 pathway, apoptosis, mTORC1 signaling, TNF-α signaling via NF-κB, and UV response. The only significantly discordant result was enrichment of oxidative phosphorylation in *Foxp1* cTG RPCs and depletion in *Jarid2* CKO RPCs. Thus, we find that

Jarid2 and *Foxp1* similarly regulate gene signatures of proliferation, biological pathways, cell signaling, and DNA damage.

DISCUSSION

Here, we report that temporal progression of CNS progenitors in developing retina is regulated by Jarid2-mediated repression of a subset of genes expressed in early progenitors, most notably *Foxp1*, which we show functions as a key effector of Jarid2-dependent regulation of temporal patterning. We thus define an important *in vivo* role for *Jarid2* in facilitating a transition in neural progenitor competence.

H3K27me3 levels are highly dynamic across retinal development,[29] and we found that loss of *Jarid2* results in a selective decrease in H3K27me3 and derepression of a subset of genes active in early RPCs. This derepression was detected at E18.5, after the transition to late RPCs. Prior evidence suggests that Jarid2 may play a role in targeting active genes for repression. For example, Jarid2/PRC2.2 is required for *de novo* silencing of genes active in ESCs, during differentiation to neural progenitor cells *in vitro*.[39] In addition, Jarid2, together with Aebp2, can partially overcome inhibition of PRC2 methyltransferase activity caused by activation marks such as H3K4me3 and H3K36me3.[38] Jarid2 has also been shown to facilitate H3K9 methylation to promote silencing of the *Notch1* locus by SETDB1 during heart development[41] and to silence *CyclinD1* via G9a/GLP,[42] so it is possible that additional Jarid2-mediated histone modifications contribute to silencing of early RPC genes during retinal development, potentially in concert with H3K27me3-mediated repression.[63] Overall, our findings show that Jarid2 promotes selective repression of subsets of active genes and a shift in gene expression during temporal pattering of progenitors to promote the change in production from early to late retinal cell types.

We identified *Foxp1* as a critical target of Jarid2-mediated polycomb repression, since it was upregulated in *Jarid2* mutant RPCs at E18.5 and showed significant reduction in H3K27me3 across the locus. *Foxp1* is notable, since its expression is highest at embryonic stages of retina development,[58] and scRNA-seq analysis has identified it as a gene enriched in early RPCs.[11] *Foxp1* encodes a transcription factor of the forkhead box (FOX) family that is expressed in developing CNS, with mutations linked to neurodevelopmental disorders.[64] During normal retinal development, we observed little H3K27me3 at the *Foxp1* locus at E14.5, when the gene is actively expressed in early RPCs, but saw acquisition of H3K27me3 by birth when the gene is silenced in late RPCs. This is consistent with prior ChIP-seq analysis showing progressive increase in H3K27me3 at the *Foxp1* locus from E17.5 to P3,[29] coincident with the progressive reduction of *Foxp1* expression in RPCs.[11,58] It is also possible that changes in the cell composition of the retina contributes to changes in H3K27me3 since the CUT&RUN analysis was performed on total retina. But, together with scRNA-seq analysis, our findings suggest that silencing of *Foxp1* expression in RPCs is facilitated by Jarid2-mediated repression, although other regulatory and transcriptional mechanisms likely contribute.[13,29]

We further establish *Foxp1* as a key competence factor for early retinal cell genesis. We first showed that *Foxp1* plays a role in early retinal cell specification, since RGCs, cones,

and horizontal cells were reduced in *Foxp1* cKO retina. A prior study did not report a visible change in retinal neurogenesis with Dkk3-Cre-mediated conditional knockout of *Foxp1*, potentially due to differences in Cre drivers used or stage of analysis resulting in a more subtle phenotype. They did report that overexpression of *Foxp1* resulted in increased cones and reduced rods, consistent with our findings.[58] Other related forkhead family transcription factors (Foxp2,4) are also expressed in the developing retina, raising the possibility of compensation by these other factors, although *Foxp1* is the most highly expressed during early development.[58] We found that elevated expression of *Foxp1*, using an inducible transgene, phenocopied the loss of *Jarid2*, resulting in enhanced production of multiple early cell types and reduced generation of late cell types such as bipolar cells and rod photoreceptors. For both loss of *Jarid2* and upregulation of *Foxp1*, this was due to extended production of early cell types. This parallels the role of *Foxp1* during cortex development, where its expression in apical radial glia during early cortical neurogenesis acts to gate the window for production of early-born deep layer neurons.[57] We found a dose-dependent effect of *Foxp1*, with two copies of the transgene promoting even higher levels of RGC differentiation, consistent with *Foxp1* levels being highest early when RGCs are being produced then gradually declining. Notably, we found that loss of *Jarid2* or elevation of *Foxp1* expression resulted in enhanced cell-cycle exit of progenitors, which is in contrast to the effects of *Foxp1* in promoting self-renewal and maintenance of apical radial glia during cortex development, suggesting potential context-dependent functions.[57] Despite divergent effects on progenitor cell proliferation, our findings suggest a conserved role for *Foxp1* in CNS progenitors in regulating the period of early neurogenesis.

RNA-seq analysis at E16.5, during the period of early cell generation, revealed that loss of *Foxp1* resulted in upregulation of multiple genes normally expressed in late RPCs or Müller glia, including *Sox9* and *Nfib*.[11] Conversely, scRNA-seq analysis of *Foxp1* cTG retina at P0 showed effects on RPC gene expression, with upregulation of multiple early RPC genes and downregulation of late RPC genes, including known late temporal identity genes *Casz1* and *Nfib*.[11,16,17] This raises the possibility that *Foxp1* promotes extended production of early retinal cell types by repressing genes in RPCs important for late temporal identity. This would be consistent with a repressor-decay timer mechanism for temporal progression whereby a temporal identity factor initiates expression when its repressor decays to a sufficiently low level, as in *Drosophila*,[65] with decline in *Foxp1* facilitated by Jarid2-mediated repression. Interestingly, our findings support predictions from scATAC-seq analysis revealing potential cross-regulatory gene networks involving *Foxp1* and *Nfi*.[13] Altogether, our observations support the conclusion that expression of *Foxp1* promotes early competence during retinal neurogenesis.

We provide substantial evidence that *Foxp1* functions as a primary effector in extending the early competence window after loss of *Jarid2*. *Foxp1* is upregulated in *Jarid2* cKO retina, and we find that loss of *Jarid2* or increased *Foxp1* expression can extend the window for early cell production, have similar effects on temporal patterning of RPC gene expression, and similarly regulate gene signatures of proliferation, biological pathways, cell signaling, and DNA damage. Importantly, we show that *Foxp1* acts epistatically to *Jarid2*, as loss of *Foxp1* reverses the enhanced production of early cell types observed with loss of *Jarid2* alone. In lymphoma, *Foxp1* is targeted and suppressed by *Ezh2* gain of function, suggesting

that *Foxp1* may be regulated by PRC2 in other contexts.[66] *Foxp1*:*Jarid2* double cKO mice did not show reduced early cell types as seen in *Foxp1* cKO mice alone, suggesting that additional factors may contribute to early cell generation. Several other genes also show increased expression and reduced H3K27me3 in the *Jarid2* cKO retina, including previously identified Jarid2 target genes,[45,56,67] but they are less highly expressed in RPCs (Figure S5) and are unlikely to drive transcriptional changes.

We found that, while *Foxp1* cTG showed reduced Müller glia number and mislocalization, *Jarid2* cKO did not affect Müller glia development. This is potentially due to more modest levels of *Foxp1* upregulation with loss of *Jarid2* than with transgenic *Foxp1* misexpression. Consistent with effects on Müller glia development, in *Foxp1* cTG retina we observed disruption of the outer limiting membrane with mislocated rod cells in the subretinal space, which is similar to the retinal phenotype reported for the *Dicer* conditional knockout.[23] Overall, we conclude that *Foxp1* is critical for extending the early competence window after loss of *Jarid2*, providing additional mechanistic insight into the interplay between epigenetic regulation, in this case related to histone modifications, and transcriptional regulation of temporal patterning in CNS progenitors. More generally, Jarid2-mediated repression may contribute to competence restriction, whereby late progenitors are restricted from generating earlier cell types.[8–10]

In *Drosophila* CNS, polycomb-dependent regulation restricts an early competence window for neuroblasts as they transition from motoneuron to interneuron production.[68] PRC2 also plays a role in timing of mammalian cortical neurogenesis and glial differentiation.[27,69] In retina, the late temporal factor Casz1 associates with nucleosome remodeling and deacetylase complex, and Jarid2 was also found in this Casz1 interactome suggesting potentially more direct interaction between regulators of temporal identity.[17] Based on our findings, it will be interesting to explore how *Jarid2* contributes to these diverse roles. While multiple mechanisms likely converge to modulate regulation of temporal patterning in neural progenitors, we propose that dynamic regulation of H3K27me3 by Jarid2 plays a role in restricting progenitor cell competence.

Limitations of the study

During the course of development,[7] or as a consequence of genetic manipulation such as *Jarid2* cKO or *Foxp1* cTG, there are changes in the proportion of different retinal cell populations. While our scRNA-seq analysis revealed gene expression changes within RPCs, we were only able to perform the CUT&RUN analysis for H3K27me3 on bulk retina, so changes in histone modification could be in part due to changes in cell composition. In addition, while loss of *Jarid2* resulted in derepression of *Foxp1*, we were not able to show Jarid2 binding to the *Foxp1* locus, despite testing several antibodies, so it remains possible that the effect on *Foxp1* repression is indirect.

RESOURCE AVAILABILITY

Lead contact—Further information and requests for resources and reagents should be directed to and will be fulfilled by the lead contact, Monica Vetter (monica.vetter@neuro.utah.edu).

Materials availability—This study did not generate new unique reagents.

Data and code availability

- All raw and processed bulk RNA-seq, single cell RNA-seq, and CUT&RUN data generated for this study have been deposited at GEO and are publicly available as of the date of publication. Accession numbers are listed in the key resources table. Additionally, this paper analyzes existing, publicly available data and the accession numbers for these datasets are listed in the key resources table.
- This paper does not report original code.
- Any additional information required to reanalyze the data reported in this paper is available from the lead contact upon request.

EXPERIMENTAL MODEL AND SUBJECT DETAILS

Mouse strains—The heterozygous *Jarid2* knockout first (KO-first) mouse line carrying a *Jarid2* KO-first allele was generated in the University of Utah Transgenic and Gene Targeting Core using cryo-archived embryos of *Jarid2*$^{tm1a(KOMP)Wtsi}$ from KOMP Repository (RRID: MMRRC:048262-UCD). The *Jarid2* floxed mice were generated by crossing *Jarid2* KO-first mice with B6.Cg-Tg(ACTFLPe) 9205Dym/J mice (RRID: IMSR_JAX:005703) which express flippase (Flp) recombinase to delete the FRT flanked trapping cassette (see Figure S1).

In order to generate retinal *Jarid2* conditional knockout (cKO), *Jarid2* floxed mice were crossed with *Six3-Cre* (RRID: IMSR_JAX:019755)[52] or *Rax-CreER*^{T2} (RRID: IMSR_JAX:025521).[53] For *Rax-CreER*^{T2} animals, Cre activity was induced by intraperitoneal injection of 75 μg Tamoxifen per gram of body weight to pregnant females at E10.5. Tamoxifen was dissolved in corn oil (Sigma-Aldrich, C8267) at a concentration of 10 mg/ml. *Foxp1* floxed (RRID: IMSR_JAX:017699) and *Foxp1a* transgenic mice (MGI:5607369) were crossed with *Six3-Cre* mice[52] to generate *Six3-Cre*; *Foxp1*$^{fl/fl}$ and *Six3-Cre*; *Foxp1*$^{tg/+}$ mice, respectively. To generate *Foxp1*:*Jarid2* double conditional knockout mice, *Foxp1*$^{fl/fl}$ mice were crossed with *Six3-Cre*; *Jarid2*$^{fl/fl}$.

The morning a plug was detected was considered embryonic day 0.5. All animals were treated within the guidelines of the University of Utah Institutional Animal Care and Use Committee (IACUC) and all experiments were IACUC approved. Both male and female animals were used unless otherwise stated.

METHOD DETAILS

Western blot—Freshly dissected retinal tissue at P0 was homogenized in lysis buffer with HaltProtease Inhibitor Cocktail (ThermoFisher 87786). Protein concentration was determined using BCA (Millipore Sigma B9643–1L). Protein was separated on Bio-Rad Mini-protean TGX Gels 4–20% (Bio-Rad 456–1093) and transferred using Bio-Rad Trans-Blot Turbo Transfer Pack (Bio-Rad 1704156). Membranes were then incubated with the primary antibodies followed by HRP conjugated secondary antibodies, and detection with Clarity Western ECL Substrate (Bio Rad 1705060).

Tissue processing—For embryonic and P0 retinal cryostat sectioning, whole heads were collected. For P10/P14 retinal cryostat sections, eyeballs were enucleated from euthanized mice and the dorsal eye marked by a cauterizer. Tissue was pre-fixed in 4% PFA for 15 minutes and a small incision was made on the cornea. Tissue was further fixed in 4% PFA for 30 minutes, washed 3 times for 20 minutes in PBS, then submerged in 10% and 20% sucrose in PBS at 4°C. Tissue was embedded in OCT compound (Tissue-Tek, Cat #27050) and stored at −80°C. Coronal cryostat sections were made at 16 μm thickness and later processed for RNA *in situ* hybridization and immunostaining with antibodies listed in the table as previously described.[35]

EdU incorporation—Pregnant females were given intraperitoneal injection of EdU (2μl 10mM EdU/gram of body weight, Invitrogen #C10637) at specific time points as indicated in the figure legends. EdU staining was performed on cryostat section using Click-iT plus EdU Imaging Kits (Invitrogen 10637 and 10640) prior to immunostaining with antibodies.

Confocal microscopy—Confocal images were acquired on an inverted Nikon A1R Confocal Microscope. Images were acquired at 20X objective with a 3X digital zoom to obtain a 0.2 μm pixel resolution. Stacks through the Z plane were taken at 0.8 μm step distance through at total of about 16 μm, covering the entire thickness of the retina. Image acquisition settings were consistent across ages and genotypes.

RT-PCR—Total RNA was isolated from freshly dissected P0 retina using RNeasy Plus Mini Kit. cDNA was synthesized using SuperScript III first-strand synthesis superMix (Invitrogen 11,752–050) followed by PCR reaction using forward (AGTTGACTCTTCTGCTCGCAC) and reverse (CTCGACGGCCCTTCTTCAAA) primers (Figure S1C). After agarose gel electrophoresis, expected bands were excised and purified before DNA sequencing.

Bulk RNA sequencing—For bulk RNA-seq analysis of *Foxp1* cKO, total RNA from E16.5 retinas was isolated using RNeasy Plus Mini Kit. Three biological replicates of each: *Six3-Cre*; $Foxp1^{fl/fl}$ animals and $Foxp1^{fl/fl}$ controls, all from the same litter, were used for RNA sequencing.

Library generation, sequencing, and alignment were performed by the Huntsman Cancer Institute High-Throughput Genomics and Bioinformatics Analysis Shared Resource. Total RNA concentration and quality were measured by RNA ScreenTape Assay (Agilent Technologies, 5067–5576, 5067–5577). All samples had a RIN value of 9.9 or better. The NEBNext Ultra II Directional RNA Library Prep Kit for Illumina with NEBNext rRNA Depletion Kit v2 (E7400) was used to generate libraries which were qualified by D1000 ScreenTape Assay (Agilent Technologies, 5067–5582, 5067–5583) and quantified with a Kapa Library Quant Kit (Kapa Biosystems, KK4824). Samples were sequenced on an Illumina NovaSeq 6000 instrument using the NovaSeq XP workflow (20043131). A 150 × 150 cycle paired end sequence run was performed using a NovaSeq 6000 S4 reagent Kit v1.5 (20028312).

To clean up the sequencing data for analysis, overlapping reads were grouped by BBTools v38.34 clumpify script,[70] specified to remove duplicate reads and optical duplicates at a max

distance of 12000. Illumina adapters were trimmed with cutadapt v2.8[71] using a minimum read length of 20 and minimum overlap between read and adaptor of 6, then aligned to mouse Ensembl genome annotation release 102 with STAR v2.7.6a in two pass mode.[72] Reads were assigned to the target that had the largest overlap and uniquely aligned, reverse stranded, reads were counted with featureCounts v1.5.1.[73] Genes with fewer than 5 counts in every sample were eliminated and differentially expressed genes were identified using DESeq2 v1.32.0.[74] In addition to the variable of interest: genotype, the additional variable: sex, was included in the DESeq2 design formula to mitigate its effect on the results.

Single cell library preparation and sequencing—For single cell analysis of *Jarid2* cKO, cells were obtained from two E18.5 tamoxifen-treated female littermates with the genotypes *Jarid*$^{fl/fl}$; *Rax-CreER*^{T2} (cKO) and *Jarid*$^{fl/fl}$ (control). For single cell analysis in *Foxp1* cTG, P0 retinas from female littermates with the genotypes *Foxp1*$^{tg/+}$; *Six3-Cre* (*Foxp1* cTG) and *Foxp1*$^{tg/+}$ (control) were used. For each sample, two freshly dissected retinas from one individual animal were pooled and dissociated in PBS, 50 mM HEPES, 0.05 mg/ml DNase I and 0.025 mg/ml Liberase for 35 min with intermediate trituration. Cells were passed through a 40 μm nylon cell strainer, washed with washing buffer (1X PBS, 2% BSA, 0.1% sodium azide, 0.05% EDTA), and red blood cells were lysed in RBC lysis buffer. Cell counts were determined using a Countess. 1× 10^6 cells was resuspended in 1mL DPBS and provided to the High Throughput Genomics Core for library prep. This protocol was repeated on different days to provide cells for Jarid2 batch I, Jarid2 batch II and Foxp1 cTG.

Single cell libraries were generated with Single Cell 3′ Gene Expression Library Prep v3 reagents for batch I and Next GEM Single Cell 3′ Gene Expression Library prep v3.1 with UDI for batch II, according to manufacturer's protocol (10X Genomics PN-1000092 and PN-1000128). Sequencing libraries were applied to a NovaSeq flow cell using XP chemistry workflow v1 and v1.5 for batch I and batch II samples respectively (Illumina 20,021,021664 and 20043131). A 150 × 150 cycle paired end sequence run was performed using an Illumina NovaSeq 6000 instrument and NovaSeq S2 reagent Kit for batch I or S4 reagent Kit v1.5 for batch II (Illumina 20012860 and 20028312). Batch I libraries were sequenced in two separate runs to a read depth of > 600 million reads per sample. Batch II libraries were sequenced to > 200 million reads per sample in a single run. Single cell library for Foxp1 cTG was prepared using the same protocol as Jarid2 batch II.

Analysis of single cell RNA-seq data—Single cell RNA-seq data was processed with the CellRanger software from 10X genomics. Briefly, sequencing reads from the Jarid2 experiment were aligned to the mm10 reference genome provided by 10X genomics (version 2020-A from Ensembl 98) while reads from Foxp1 experiment were aligned to a reference including the mm10 genome, GFP, and Cre. Feature-barcode matrices were generated using cellranger count v3.1.0 with expected-cells set to 5000. Spliced and unspliced transcripts counts were also generated from Jarid2 batch II single cell samples with velocyto v0.17.17.[75] Total transcripts were used for all analyses unless specified otherwise.

Filtered feature matrices from CellRanger were further filtered with the aid of Seurat v4.0.3. High quality cells were identified by a mitochondrial percentage <7.5 and a high number

of genes/features. The feature cut-off was determined independently for each sample by the local minimum cell density between 200 and 2000 features (con I = 1490, cKO I = 1845, con II = 1367, cKO II = 1481. Foxp1 con = 1000, Foxp1 cTG = 1050). Each sample was run, individually, through Seurat's SCTransform pipeline, regressing out mitochondrial percentage, to generate unsupervised cell clusters. For Jarid2 samples DoubletFinder v2.0.3 identified likely doublets assuming 0.8% doublets in 1000 cells, adjusted for homotypic doublets.[76] Doublets were excluded from downstream analysis.

Jarid2 batch I and batch II were combined into a single dataset using the Seurat's integration anchor pipeline with principal components set to 30 and cluster resolution to 2.[81] Foxp1 cTG single cell samples were combined with the merge function. Clusters were manually annotated using expression of known cell markers: *Vsx2*, *Lhx2*, and *Pax6* for RPCs, *Neurog2* and *Olig2* for neurogenic cells, *Crx* for photoreceptor precursors, *Thrb* for cones, *Nrl* for rods, *Rbpms* for retinal ganglion cells, *Tfap2a* for amacrine cells, and *Lhx1* for horizontal cells. Differential expression analysis was performed with Seurat FindMarkers, using logfc.threshold of 0.1. For Foxp1 cTG, markers were further narrowed by q-value <0.01. Using Jarid2 batch II samples only, the SCTranform pipeline was run on spliced transcripts, regressing out cell cycle scores, to obtain a UMAP representing mature transcriptional state. Cell type annotation for the spliced UMAP was carried over from the integrated dataset.

Gene set enrichment analysis was run on RPC gene expression from the *Jarid2* cKO dataset and *Foxp1* cTG dataset sperately using gene sets obtained from the Molecular Signatures Database.[82] Specifically, we used the mouse-ortholog hallmark gene sets v2022.1. All detectable genes were ranked by average log2 fold change between *Jarid2* control and cKO or between *Foxp1* control and cTG, and analyzed with both fgsea v1.18.0[79] and gage v2.42.0[80] using default settings. We only marked gene sets as significant if they were significantly changed, in the same direction, by both methods. Q-values listed are from fgsea results.

Gene module analysis—To identify gene modules that vary across development, we utilized single cell sequencing data from whole retina across from E11 to P5[11] (GEO: GSE118614). Retinal progenitor cells, as defined in that study were analyzed with Seurat's SCTransform function followed by dimensional reduction, with cell cycle differences and mitochondrial percentage regressed out of the model. Highly variable features, identified from the retinal progenitor cells, were grouped into 22 modules with Monocle functions.[55] Normalized counts were summed for the genes in each module at each age, and scaled across the modules. Only those modules that varied across development, with a standard deviation range >1.25, were selected to display. We also eliminated module 22 for being driven by red blood cell transcripts. Separately, gene expression was aggregated from control and Jarid2 cKO RPCs across these same modules. These data were combined, and values were scaled across each age or condition to generate a heatmap and dendrogram. Hierarchical clustering was performed with hclust using method ward.D2.

CUT&RUN sample and library preparation—The H3K27me3 CUT&RUN was performed in two separate batches. In batch I, two biological replicates were used for control

(*Jarid2*$^{fl/fl}$) and conditional knockout (*Rax-CreER*^{T2}; *Jarid2*$^{fl/fl}$), one male and one female of each genotype, all from a single litter. Batch II consisted of all male littermates: three biological replicates, each with two technical duplicates, for a total of 12 samples. Single cell suspensions were made using the same method described for single cell sequencing. CUT&RUN[83] was performed using a CUT&RUN Assay Kit according to manufacturer's protocol. 300K single cells were used for each reaction. 2 μl rabbit anti-H3K27me3 antibody was used for H3K27me3 Immunoprecipitation. This antibody has been validated for specificity by ENCODE.[84,85] 5 μl Rabbit I (DA1E) mAb IgG XP Isotype Control provided by the kit was used as a negative control. DNA fragments were purified on spin columns, eluted with 50 μl buffer (Cell Signaling 14209) and provided to University of Utah High Throughput Genomics Core for library generation.

DNA quality was confirmed by PCR, libraries were created with the NEBNext UItra II DNA Library Prep Kit (New England Biolabs E7645S), and 150 bp paired-end sequencing was performed on a NovaSeq 6000 using the XP chemistry workflow (20021664) and S4 reagent Kit v1.5 (20028312).

CUT&RUN data analysis—All CUT&RUN samples were aligned to mouse genome build mm10 with Novoalign v4.02.02 using standard Illumina TruSeq adapters. Samtools fixmate v1.10[77] removed unmapped reads and added mate scores, then bam files were sorted and indexed. Unique Molecular Indexes (UMIs) were sequenced to identify PCR duplicates, and the UMIs were handled by scripts written by the Huntsman Cancer Institute Bioinformatics Core. PCR and optical duplicates were removed with optical distance threshold at 2500. H3K27me3 broad peak calling was done with a Macs2-based pipeline,[78] MultiRepMacsChIPSeq v17.7, developed by the University of Utah Bioinformatics Shared Resource (github.com/HuntsmanCancerInstitute/MultiRepMacsChIPSeq). Briefly, multirep_macs2_pipeline.pl was run with the following parameters: q-value threshold for peak calling set to 2, minimum peak size of 600, maximum gap size of 300, minimum mapping quality of 10, q-value cutoff of 0.1, maximum link size of 1500 and mappable genome size 2500000000,. The output of this pipeline includes fragment tracks, log2 fold enrichment of H3K27me3 relative to IgG, identification of called peaks, annotation with Ensembl release 102, and counts of fragments in each peak. Difference calling between control and *Jarid2* cKO was done with DESeq2 v1.38.1, controlling for batch effect.

Wild type E14.5 and P0 CUT&RUN samples were prepared, sequenced and analyzed as described above, with the following specific changes: P0 H3K27me3 and P0 IgG samples were run in technical triplicate, E14.5 H3K27me3 was run in duplicate, and E14.5 IgG was a single sample. Only female pups were used to perform CUT&RUN for H3K27me3, and IgG. Samples were purified on DNA spin column (cell signaling #14209) and eluted with 35 μL elution buffer. 5 μL was used for PCR to validate sample quality and the rest used for library preparation. PCR showed specific bands with positive control primers for H3K27me3. MultiRepMacsChIPSeq was run with expected fragment size of 200 to obtain fragment and log2 fold enrichment tracks of H3K27me3 relative to IgG at E14.5 and P0.

For developmental time-course comparison, we obtained fastq files from[29] (GEO: GSE87037). Specifically, input samples and ChIP-seq targeting H3K27me3 in whole murine

retina at E17.5, P0 and P3 were used. Alignment to mm10 was performed as described above except that, as these are single-read samples, a mate score was not added. Broad H3K27me3 peaks were called for each replicate with the MultiRepMacsChIPSeq pipeline run as above with specific changes: no optical distance set and duplication rate set to 5%. Peaks from individual samples were merged into a single bed file for counting, and differential peak enrichment was done with DESeq2.

QUANTIFICATION AND STATISTICAL ANALYSIS—Confocal images shown are representative of at least 3 animals/6 retinas. For quantification, the number of retinal cells was quantified manually and blindly by averaging total positive cells within the central retinal region (~300 μm length) from 4–5 sections per retina using Nikon Elements software. For EdU birthdating analysis, the number of cells colocalizing EdU with different retinal markers was counted within the central retinal region (~1000 μm length) and averaged per retina. For cell-cycle exit analysis, EdU was injected 24 h before retina collection. Total EdU+ cells and EdU+PCNA-cells were counted within the central retinal region (~300 μm length) and the cell-cycle exit index was calculated as EdU+PCNA−/total EdU+.[86] The index was then averaged from 3–4 sections per retina.

Statistical analysis was performed on all image data using GraphPad Prism software and the details (p values, sample sizes and statistical methods) can be found in Table S6. The sample size (n) is the number of experimental units which represents individual eyes. In each experiment, the sample size was determined to meet the criteria that statistical power would be more than 80% with the use of a two-tailed unpaired t test at the significance level (p value) of 0.05. All graph data are presented as mean ± standard error of the mean (SEM). In all graphs, dots represent individual retina. *p < 0.05; **p < 0.01; ***p < 0.001; ****p < 0.0001. ns = not significant.

Supplementary Material

Refer to Web version on PubMed Central for supplementary material.

ACKNOWLEDGMENTS

This research was supported by the National Eye Institute award R01EY012274 (to M.L.V.). We thank Madelyn Lee for technical assistance. We thank Richard Dorsky, Issam Al Diri, Sarah Anderson, Mariana S. Silveira, Viviane Valenca, and Brad Cairns for providing comments on the manuscript. We thank Seth Blackshaw for providing *Rax-CreER*^{T2} mice and Hui Hu for providing *Foxp1a* transgenic mice. We thank the University of Utah Office of Comparative Medicine for animal husbandry. Research reported in this publication utilized the High-Throughput Genomics and Bioinformatic Analysis Shared Resource at Huntsman Cancer Institute in the University of Utah and was supported by the National Cancer Institute of the National Institutes of Health under award no. P30CA042014. The computational resources used were partially funded by the NIH Shared Instrumentation grant 1S10OD021644-01A1. Sanger DNA sequencing was performed at the DNA Sequencing Core Facility, University of Utah. The content is solely the responsibility of the authors and does not necessarily represent the official views of the NIH.

REFERENCES

1. Holguera I, and Desplan C. (2018). Neuronal specification in space and time. Science 362, 176–180. 10.1126/science.aas9435. [PubMed: 30309944]
2. Rossi AM, Fernandes VM, and Desplan C. (2017). Timing temporal transitions during brain development. Curr. Opin. Neurobiol 42, 84–92. 10.1016/j.conb.2016.11.010. [PubMed: 27984764]

3. Adam MA, and Harwell CC (2020). Epigenetic regulation of cortical neurogenesis; orchestrating fate switches at the right time and place. Curr. Opin. Neurobiol 63, 146–153. 10.1016/j.conb.2020.03.012. [PubMed: 32428815]
4. Bonnefont J, and Vanderhaeghen P. (2021). Neuronal fate acquisition and specification: time for a change. Curr. Opin. Neurobiol 66, 195–204. 10.1016/j.conb.2020.12.006. [PubMed: 33412482]
5. Cepko C. (2014). Intrinsically different retinal progenitor cells produce specific types of progeny. Nat. Rev. Neurosci 15, 615–627. 10.1038/nrn3767. [PubMed: 25096185]
6. Ray A, Zhu H, Ding A, and Li X. (2022). Transcriptional and epigenetic regulation of temporal patterning in neural progenitors. Dev. Biol 481, 116–128. 10.1016/j.ydbio.2021.10.006. [PubMed: 34666024]
7. Petridou E, and Godinho L. (2022). Cellular and molecular determinants of retinal cell fate. Annu. Rev. Vis. Sci 8, 79–99. 10.1146/annurev-vision-100820-103154. [PubMed: 36108104]
8. Mattar P, and Cayouette M. (2015). Mechanisms of temporal identity regulation in mouse retinal progenitor cells. Neurogenesis (Austin) 2, e1125409. 10.1080/23262133.2015.1125409. [PubMed: 27606333]
9. Belliveau MJ, Young TL, and Cepko CL (2000). Late retinal progenitor cells show intrinsic limitations in the production of cell types and the kinetics of opsin synthesis. J. Neurosci 20, 2247–2254. [PubMed: 10704500]
10. Cayouette M, Barres BA, and Raff M. (2003). Importance of intrinsic mechanisms in cell fate decisions in the developing rat retina. Neuron 40, 897–904. 10.1016/s0896-6273(03)00756-6. [PubMed: 14659089]
11. Clark BS, Stein-O'Brien GL, Shiau F, Cannon GH, Davis-Marcisak E, Sherman T, Santiago CP, Hoang TV, Rajaii F, James-Esposito RE, et al. (2019). Single-cell RNA-seq analysis of retinal development identifies NFI factors as regulating mitotic exit and late-born cell specification. Neuron 102, 1111–1126.e5. 10.1016/j.neuron.2019.04.010. [PubMed: 31128945]
12. Lu Y, Shiau F, Yi W, Lu S, Wu Q, Pearson JD, Kallman A, Zhong S, Hoang T, Zuo Z, et al. (2020). Single-cell analysis of human retina identifies evolutionarily conserved and species-specific mechanisms controlling development. Dev. Cell 53, 473–491.e9. 10.1016/j.devcel.2020.04.009. [PubMed: 32386599]
13. Lyu P, Hoang T, Santiago CP, Thomas ED, Timms AE, Appel H, Gimmen M, Le N, Jiang L, Kim DW, et al. (2021). Gene regulatory networks controlling temporal patterning, neurogenesis, and cell-fate specification in mammalian retina. Cell Rep. 37, 109994. 10.1016/j.celrep.2021.109994. [PubMed: 34788628]
14. Elliott J, Jolicoeur C, Ramamurthy V, and Cayouette M. (2008). Ikaros confers early temporal competence to mouse retinal progenitor cells. Neuron 60, 26–39. 10.1016/j.neuron.2008.08.008. [PubMed: 18940586]
15. Liu S, Liu X, Li S, Huang X, Qian H, Jin K, and Xiang M. (2020). Foxn4 is a temporal identity factor conferring mid/late-early retinal competence and involved in retinal synaptogenesis. Proc. Natl. Acad. Sci. USA 117, 5016–5027. 10.1073/pnas.1918628117. [PubMed: 32071204]
16. Mattar P, Ericson J, Blackshaw S, and Cayouette M. (2015). A conserved regulatory logic controls temporal identity in mouse neural progenitors. Neuron 85, 497–504. 10.1016/j.neuron.2014.12.052. [PubMed: 25654255]
17. Mattar P, Jolicoeur C, Dang T, Shah S, Clark BS, and Cayouette M. (2021). A Casz1-NuRD complex regulates temporal identity transitions in neural progenitors. Sci. Rep 11, 3858. 10.1038/s41598-021-83395-7. [PubMed: 33594190]
18. Javed A, Mattar P, Lu S, Kruczek K, Kloc M, Gonzalez-Cordero A, Bremner R, Ali RR, and Cayouette M. (2020). Pou2f1 and Pou2f2 Cooperate to Control the Timing of Cone Photoreceptor Production in the Developing Mouse Retina. Development 147. 10.1242/dev.188730.
19. Javed A, Santos-França PL, Mattar P, Cui A, Kassem F, and Cayouette M. (2023). Ikaros family proteins redundantly regulate temporal patterning in the developing mouse retina. Development 150, dev200436. 10.1242/dev.200436.
20. La Torre A, Georgi S, and Reh TA (2013). Conserved microRNA pathway regulates developmental timing of retinal neurogenesis. Proc. Natl. Acad. Sci. USA 110, E2362–E2370. 10.1073/pnas.1301837110. [PubMed: 23754433]

21. Decembrini S, Andreazzoli M, Barsacchi G, and Cremisi F. (2008). Dicer inactivation causes heterochronic retinogenesis in Xenopus laevis. Int. J. Dev. Biol 52, 1099–1103. 10.1387/ijdb.082646sd. [PubMed: 18956342]
22. Decembrini S, Bressan D, Vignali R, Pitto L, Mariotti S, Rainaldi G, Wang X, Evangelista M, Barsacchi G, and Cremisi F. (2009). MicroRNAs couple cell fate and developmental timing in retina. Proc. Natl. Acad. Sci. USA 106, 21179–21184. 10.1073/pnas.0909167106. [PubMed: 19965369]
23. Georgi SA, and Reh TA (2010). Dicer is required for the transition from early to late progenitor state in the developing mouse retina. J. Neurosci 30, 4048–4061. 10.1523/JNEUROSCI.4982-09.2010. [PubMed: 20237275]
24. Gordon PJ, Yun S, Clark AM, Monuki ES, Murtaugh LC, and Levine EM (2013). Lhx2 balances progenitor maintenance with neurogenic output and promotes competence state progression in the developing retina. J. Neurosci 33, 12197–12207. 10.1523/JNEUROSCI.1494-13.2013. [PubMed: 23884928]
25. Zibetti C, Liu S, Wan J, Qian J, and Blackshaw S. (2019). Epigenomic profiling of retinal progenitors reveals LHX2 is required for developmental regulation of open chromatin. Commun. Biol 2, 142. 10.1038/s42003-019-0375-9. [PubMed: 31044167]
26. Yoon KJ, Vissers C, Ming GL, and Song H. (2018). Epigenetics and epitranscriptomics in temporal patterning of cortical neural progenitor competence. J. Cell Biol 217, 1901–1914. 10.1083/jcb.201802117. [PubMed: 29666150]
27. Pereira JD, Sansom SN, Smith J, Dobenecker MW, Tarakhovsky A, and Livesey FJ (2010). Ezh2, the histone methyltransferase of PRC2, regulates the balance between self-renewal and differentiation in the cerebral cortex. Proc. Natl. Acad. Sci. USA 107, 15957–15962. 10.1073/pnas.1002530107. [PubMed: 20798045]
28. Raeisossadati R, Ferrari MFR, Kihara AH, AlDiri I, and Gross JM (2021). Epigenetic regulation of retinal development. Epigenet. Chromatin 14, 11. 10.1186/s13072-021-00384-w.
29. Aldiri I, Xu B, Wang L, Chen X, Hiler D, Griffiths L, Valentine M, Shirinifard A, Thiagarajan S, Sablauer A, et al. (2017). The dynamic epigenetic landscape of the retina during development, reprogramming, and tumorigenesis. Neuron 94, 550–568.e10. 10.1016/j.neuron.2017.04.022. [PubMed: 28472656]
30. Margueron R, and Reinberg D. (2011). The Polycomb complex PRC2 and its mark in life. Nature 469, 343–349. 10.1038/nature09784. [PubMed: 21248841]
31. Liu PP, Xu YJ, Teng ZQ, and Liu CM (2018). Polycomb repressive complex 2: emerging roles in the central nervous system. Neuroscientist 24, 208–220. 10.1177/1073858417747839. [PubMed: 29283025]
32. Jambhekar A, Dhall A, and Shi Y. (2019). Roles and regulation of histone methylation in animal development. Nat. Rev. Mol. Cell Biol 20, 625–641. 10.1038/s41580-019-0151-1. [PubMed: 31267065]
33. Fujimura N, Kuzelova A, Ebert A, Strnad H, Lachova J, Machon O, Busslinger M, and Kozmik Z. (2018). Polycomb repression complex 2 is required for the maintenance of retinal progenitor cells and balanced retinal differentiation. Dev. Biol 433, 47–60. 10.1016/j.ydbio.2017.11.004. [PubMed: 29137925]
34. Iida A, Iwagawa T, Kuribayashi H, Satoh S, Mochizuki Y, Baba Y, Nakauchi H, Furukawa T, Koseki H, Murakami A, and Watanabe S. (2014). Histone demethylase Jmjd3 is required for the development of subsets of retinal bipolar cells. Proc. Natl. Acad. Sci. USA 111, 3751–3756. 10.1073/pnas.1311480111. [PubMed: 24572572]
35. Zhang J, Taylor RJ, La Torre A, Wilken MS, Cox KE, Reh TA, and Vetter ML (2015). Ezh2 maintains retinal progenitor proliferation, transcriptional integrity, and the timing of late differentiation. Dev. Biol 403, 128–138. 10.1016/j.ydbio.2015.05.010. [PubMed: 25989023]
36. van Mierlo G, Veenstra GJC, Vermeulen M, and Marks H. (2019). The complexity of PRC2 subcomplexes. Trends Cell Biol. 29, 660–671. 10.1016/j.tcb.2019.05.004. [PubMed: 31178244]
37. Højfeldt JW, Hedehus L, Laugesen A, Tatar T, Wiehle L, and Helin K. (2019). Non-core subunits of the PRC2 complex are collectively required for its target-site specificity. Mol. Cell 76, 423–436.e3. 10.1016/j.molcel.2019.07.031. [PubMed: 31521506]

38. Kasinath V, Beck C, Sauer P, Poepsel S, Kosmatka J, Faini M, Toso D, Aebersold R, and Nogales E. (2021). JARID2 and AEBP2 regulate PRC2 in the presence of H2AK119ub1 and other histone modifications. Science 371, eabc3393. 10.1126/science.abc3393.
39. Petracovici A, and Bonasio R. (2021). Distinct PRC2 subunits regulate maintenance and establishment of Polycomb repression during differentiation. Mol. Cell 81, 2625–2639.e5. 10.1016/j.molcel.2021.03.038. [PubMed: 33887196]
40. Youmans DT, Gooding AR, Dowell RD, and Cech TR (2021). Competition between PRC2.1 and 2.2 subcomplexes regulates PRC2 chromatin occupancy in human stem cells. Mol. Cell 81, 488–501.e9. 10.1016/j.molcel.2020.11.044. [PubMed: 33338397]
41. Mysliwiec MR, Carlson CD, Tietjen J, Hung H, Ansari AZ, and Lee Y. (2012). Jarid2 (Jumonji, AT rich interactive domain 2) regulates NOTCH1 expression via histone modification in the developing heart. J. Biol. Chem 287, 1235–1241. 10.1074/jbc.M111.315945. [PubMed: 22110129]
42. Shirato H, Ogawa S, Nakajima K, Inagawa M, Kojima M, Tachibana M, Shinkai Y, and Takeuchi T. (2009). A jumonji (Jarid2) protein complex represses cyclin D1 expression by methylation of histone H3-K9. J. Biol. Chem 284, 733–739. 10.1074/jbc.M804994200. [PubMed: 19010785]
43. Takeuchi T, Yamazaki Y, Katoh-Fukui Y, Tsuchiya R, Kondo S, Motoyama J, and Higashinakagawa T. (1995). Gene trap capture of a novel mouse gene, jumonji, required for neural tube formation. Genes Dev. 9, 1211–1222. [PubMed: 7758946]
44. Landeira D, and Fisher AG (2011). Inactive yet indispensable: the tale of Jarid2. Trends Cell Biol. 21, 74–80. 10.1016/j.tcb.2010.10.004. [PubMed: 21074441]
45. Pasini D, Cloos PAC, Walfridsson J, Olsson L, Bukowski JP, Johansen JV, Bak M, Tommerup N, Rappsilber J, and Helin K. (2010). JARID2 regulates binding of the Polycomb repressive complex 2 to target genes in ES cells. Nature 464, 306–310. 10.1038/nature08788. [PubMed: 20075857]
46. Jung J, Mysliwiec MR, and Lee Y. (2005). Roles of JUMONJI in mouse embryonic development. Dev. Dynam 232, 21–32, an official publication of the American Association of Anatomists. 10.1002/dvdy.20204.
47. Liu Y, Chen G, Norton N, Liu W, Zhu H, Zhou P, Luan M, Yang S, Chen X, Carroll L, et al. (2009). Whole genome association study in a homogenous population in Shandong peninsula of China reveals JARID2 as a susceptibility gene for schizophrenia. J. Biomed. Biotechnol 2009, 536918. 10.1155/2009/536918. [PubMed: 19884986]
48. Mo W, Liu J, Zhang Z, Yu H, Yang A, Qu F, Hu P, Liu Z, and Hu F. (2018). A study of single nucleotide polymorphisms in CD157, AIM2 and JARID2 genes in Han Chinese children with autism spectrum disorder. Nord. J. Psychiatr 72, 179–183. 10.1080/08039488.2017.1410570.
49. Pedrosa E, Ye K, Nolan KA, Morrell L, Okun JM, Persky AD, Saito T, and Lachman HM (2007). Positive association of schizophrenia to JARID2 gene. Am. J. Med. Genet. B Neuropsychiatr. Genet 144B, 45–51. 10.1002/ajmg.b.30386. [PubMed: 16967465]
50. Ramos PS, Sajuthi S, Langefeld CD, and Walker SJ (2012). Immune function genes CD99L2, JARID2 and TPO show association with autism spectrum disorder. Mol. Autism 3, 4. 10.1186/2040-2392-3-4. [PubMed: 22681640]
51. Verberne EA, Goh S, England J, van Ginkel M, Rafael-Croes L, Maas S, Polstra A, Zarate YA, Bosanko KA, Pechter KB, et al. (2021). JARID2 haploinsufficiency is associated with a clinically distinct neurodevelopmental syndrome. Genet. Med 23, 374–383. 10.1038/s41436-020-00992-z. [PubMed: 33077894]
52. Furuta Y, Lagutin O, Hogan BL, and Oliver GC (2000). Retina- and ventral forebrain-specific Cre recombinase activity in transgenic mice. Genesis 26, 130–132. [PubMed: 10686607]
53. Pak T, Yoo S, Miranda-Angulo AL, Wang H, and Blackshaw S. (2014). Rax-CreERT2 knock-in mice: a tool for selective and conditional gene deletion in progenitor cells and radial glia of the retina and hypothalamus. PLoS One 9, e90381. 10.1371/journal.pone.0090381. [PubMed: 24699247]
54. Young RW (1985). Cell differentiation in the retina of the mouse. Anat. Rec 212, 199–205. 10.1002/ar.1092120215. [PubMed: 3842042]
55. Qiu X, Mao Q, Tang Y, Wang L, Chawla R, Pliner HA, and Trapnell C. (2017). Reversed graph embedding resolves complex single-cell trajectories. Nat. Methods 14, 979–982. 10.1038/nmeth.4402. [PubMed: 28825705]

56. Peng JC, Valouev A, Swigut T, Zhang J, Zhao Y, Sidow A, and Wysocka J. (2009). Jarid2/Jumonji coordinates control of PRC2 enzymatic activity and target gene occupancy in pluripotent cells. Cell 139, 1290–1302. 10.1016/j.cell.2009.12.002. [PubMed: 20064375]
57. Pearson CA, Moore DM, Tucker HO, Dekker JD, Hu H, Miquela-jáuregui A, and Novitch BG (2020). *Foxp1* regulates neural stem cell self-renewal and bias toward deep layer cortical fates. Cell Rep. 30, 1964–1981.e3. 10.1016/j.celrep.2020.01.034. [PubMed: 32049024]
58. Suzuki-Kerr H, Baba Y, Tsuhako A, Koso H, Dekker JD, Tucker HO, Kuribayashi H, and Watanabe S. (2017). Forkhead box protein P1 is dispensable for retina but essential for lens development. Invest. Ophthalmol. Vis. Sci 58, 1916–1929. 10.1167/iovs.1620085. [PubMed: 28384713]
59. Rousso DL, Qiao M, Kagan RD, Yamagata M, Palmiter RD, and Sanes JR (2016). Two pairs of on and off retinal ganglion cells are defined by intersectional patterns of transcription factor expression. Cell Rep. 15, 1930–1944. 10.1016/j.celrep.2016.04.069. [PubMed: 27210758]
60. Feng X, Ippolito GC, Tian L, Wiehagen K, Oh S, Sambandam A, Willen J, Bunte RM, Maika SD, Harriss JV, et al. (2010). *Foxp1* is an essential transcriptional regulator for the generation of quiescent naive T cells during thymocyte development. Blood 115, 510–518. 10.1182/blood-2009-07-232694. [PubMed: 19965654]
61. Wang H, Geng J, Wen X, Bi E, Kossenkov AV, Wolf AI, Tas J, Choi YS, Takata H, Day TJ, et al. (2014). The transcription factor Foxp1 is a critical negative regulator of the differentiation of follicular helper T cells. Nat. Immunol 15, 667–675. 10.1038/ni.2890. [PubMed: 24859450]
62. Subramanian A, Tamayo P, Mootha VK, Mukherjee S, Ebert BL, Gillette MA, Paulovich A, Pomeroy SL, Golub TR, Lander ES, and Mesirov JP (2005). Gene set enrichment analysis: a knowledge-based approach for interpreting genome-wide expression profiles. Proc. Natl. Acad. Sci. USA 102, 15545–15550. 10.1073/pnas.0506580102. [PubMed: 16199517]
63. Fong KW, Zhao JC, Lu X, Kim J, Piunti A, Shilatifard A, and Yu J. (2022). PALI1 promotes tumor growth through competitive recruitment of PRC2 to G9A-target chromatin for dual epigenetic silencing. Mol. Cell 82, 4611–4626.e7. 10.1016/j.molcel.2022.11.010. [PubMed: 36476474]
64. Co M, Anderson AG, and Konopka G. (2020). FOXP transcription factors in vertebrate brain development, function, and disorders. Wiley Interdiscip Rev Dev Biol 9, e375. 10.1002/wdev.375. [PubMed: 31999079]
65. Averbukh I, Lai SL, Doe CQ, and Barkai N. (2018). A repressor-decay timer for robust temporal patterning in embryonic Drosophila neuroblast lineages. Elife 7, e38631. 10.7554/eLife.38631. [PubMed: 30526852]
66. Gan L, Yang Y, Li Q, Feng Y, Liu T, and Guo W. (2018). Epigenetic regulation of cancer progression by EZH2: from biological insights to therapeutic potential. Biomark. Res 6, 10. 10.1186/s40364018-0122-2. [PubMed: 29556394]
67. Zhao L, Li J, Ma Y, Wang J, Pan W, Gao K, Zhang Z, Lu T, Ruan Y, Yue W, et al. (2015). Ezh2 is involved in radial neuronal migration through regulating Reelin expression in cerebral cortex. Sci. Rep 5, 15484. 10.1038/srep15484. [PubMed: 26499080]
68. Touma JJ, Weckerle FF, and Cleary MD (2012). Drosophila Polycomb complexes restrict neuroblast competence to generate motoneurons. Development 139, 657–666. 10.1242/dev.071589. [PubMed: 22219354]
69. Hirabayashi Y, Suzki N, Tsuboi M, Endo TA, Toyoda T, Shinga J, Koseki H, Vidal M, and Gotoh Y. (2009). Polycomb limits the neurogenic competence of neural precursor cells to promote astrogenic fate transition. Neuron 63, 600–613. 10.1016/j.neuron.2009.08.021. [PubMed: 19755104]
70. Bushnell B, Rood J, and Singer E. (2017). BBMerge - accurate paired shotgun read merging via overlap. PLoS One 12, e0185056. 10.1371/journal.pone.0185056. [PubMed: 29073143]
71. Martin M. (2011). Cutadapt removes adapter sequences from high-throughput sequencing reads. EMBnet. j 17, 10–12.
72. Dobin A, Davis CA, Schlesinger F, Drenkow J, Zaleski C, Jha S, Batut P, Chaisson M, and Gingeras TR (2013). STAR: ultrafast universal RNA-seq aligner. Bioinformatics 29, 15–21. 10.1093/bioinformatics/bts635. [PubMed: 23104886]

73. Liao Y, Smyth GK, and Shi W. (2014). featureCounts: an efficient general purpose program for assigning sequence reads to genomic features. Bioinformatics 30, 923–930. 10.1093/bioinformatics/btt656. [PubMed: 24227677]
74. Love MI, Huber W, and Anders S. (2014). Moderated estimation of fold change and dispersion for RNA-seq data with DESeq2. Genome Biol. 15, 550. 10.1186/s13059-014-0550-8. [PubMed: 25516281]
75. La Manno G, Soldatov R, Zeisel A, Braun E, Hochgerner H, Petukhov V, Lidschreiber K, Kastriti ME, Lönnerberg P, Furlan A, et al. (2018). RNA velocity of single cells. Nature 560, 494–498. 10.1038/s41586-018-0414-6. [PubMed: 30089906]
76. McGinnis CS, Murrow LM, and Gartner ZJ (2019). DoubletFinder: doublet detection in single-cell RNA sequencing data using artificial nearest Neighbors. Cell Syst. 8, 329–337.e4. 10.1016/j.cels.2019.03.003. [PubMed: 30954475]
77. Danecek P, Bonfield JK, Liddle J, Marshall J, Ohan V, Pollard MO, Whitwham A, Keane T, McCarthy SA, Davies RM, and Li H. (2021). Twelve years of SAMtools and BCFtools. GigaScience 10, giab008. 10.1093/gigascience/giab008.
78. Zhang Y, Liu T, Meyer CA, Eeckhoute J, Johnson DS, Bernstein BE, Nusbaum C, Myers RM, Brown M, Li W, and Liu XS (2008). Model-based analysis of ChIP-seq (MACS). Genome Biol. 9, R137. 10.1186/gb-2008-9-9-r137. [PubMed: 18798982]
79. Korotkevich G, Sukhov V, Budin N, Shpak B, Artyomov MN, and Sergushichev A. (2021). Fast gene set enrichment analysis. Preprint at bioRxiv. 10.1101/060012.
80. Luo W, Friedman MS, Shedden K, Hankenson KD, and Woolf PJ (2009). GAGE: generally applicable gene set enrichment for pathway analysis. BMC Bioinf. 10, 161. 10.1186/1471-2105-10-161.
81. Stuart T, Butler A, Hoffman P, Hafemeister C, Papalexi E, Mauck WM 3rd, Hao Y, Stoeckius M, Smibert P, and Satija R. (2019). Comprehensive integration of single-cell data. Cell 177, 1888–1902.e21. 10.1016/j.cell.2019.05.031. [PubMed: 31178118]
82. Liberzon A, Birger C, Thorvaldsdóttir H, Ghandi M, Mesirov JP, and Tamayo P. (2015). The Molecular Signatures Database (MSigDB) hallmark gene set collection. Cell Syst. 1, 417–425. 10.1016/j.cels.2015.12.004. [PubMed: 26771021]
83. Skene PJ, and Henikoff S. (2017). An efficient targeted nuclease strategy for high-resolution mapping of DNA binding sites. Elife 6, e21856. 10.7554/eLife.21856. [PubMed: 28079019]
84. Davis CA, Hitz BC, Sloan CA, Chan ET, Davidson JM, Gabdank I, Hilton JA, Jain K, Baymuradov UK, Narayanan AK, et al. (2018). The Encyclopedia of DNA elements (ENCODE): data portal update. Nucleic Acids Res. 46, D794–D801. 10.1093/nar/gkx1081. [PubMed: 29126249]
85. Sloan CA, Chan ET, Davidson JM, Malladi VS, Strattan JS, Hitz BC, Gabdank I, Narayanan AK, Ho M, Lee BT, et al. (2016). ENCODE data at the ENCODE portal. Nucleic Acids Res. 44, D726–D732. 10.1093/nar/gkv1160. [PubMed: 26527727]
86. Farhy C, Elgart M, Shapira Z, Oron-Karni V, Yaron O, Menuchin Y, Rechavi G, and Ashery-Padan R. (2013). Pax6 is required for normal cell-cycle exit and the differentiation kinetics of retinal progenitor cells. PLoS One 8, e76489. 10.1371/journal.pone.0076489. [PubMed: 24073291]

Highlights

- Loss of *Jarid2* delays retinal progenitor early- to late-identity transition
- Jarid2 mediates H3K27me3 deposition and repression of early genes including *Foxp1*
- *Foxp1* regulates the timing of early retinal cell production
- *Foxp1* is an effector of *Jarid2*-mediated temporal patterning

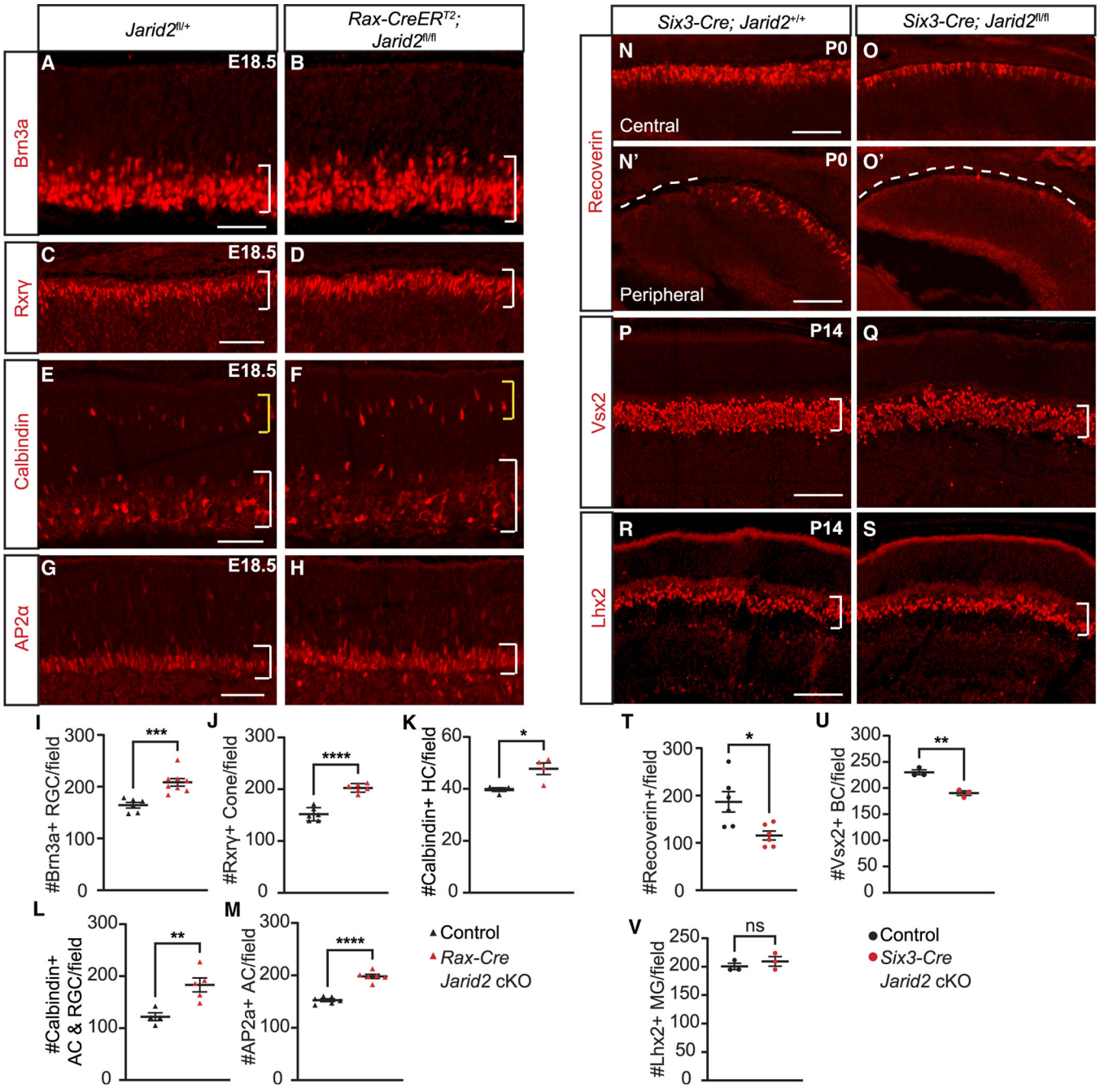

Figure 1. Loss of *Jarid2* affects retinal neurogenesis

Rax-Cre Jarid2 cKO retina at E18.5 shows (A, B, and I) increased Brn3a-labeled RGCs within the GCL (bracket), (C, D, and J) increased Rxrγ-labeled cone photoreceptors (bracket), (E and F) increased calbindin-labeled horizontal cells (yellow bracket, K) and amacrine cells (white bracket, L), and (G, H, and M) increased AP2α-labeled amacrine cells (bracket). At P0, *Six3-Cre Jarid2* cKO shows (N, O, and T) reduced Recoverin-labeled photoreceptors in the central retina (N′ and O′) and delayed differentiation in the peripheral retina (dotted line). At P14 (P, Q, and U), Vsx2-labeled bipolar cells were reduced, (R, S and V) but Lhx2-labeled Müller glia were unchanged. Graphs represent mean ± SEM. n =

6 retinas in (J, M, and T) and control in (I), n = 8 for *Jarid2* cKO in (I), n = 4 in (K), and control in (L), n = 5 for *Jarid2* cKO in (L), and n = 3 in (U and V). *p < 0.05, **p < 0.01, ***p < 0.001, ****p < 0.0001 by Student's t test. Scale bars, 100 μm. See also Figure S2 and Table S6 for statistical details.

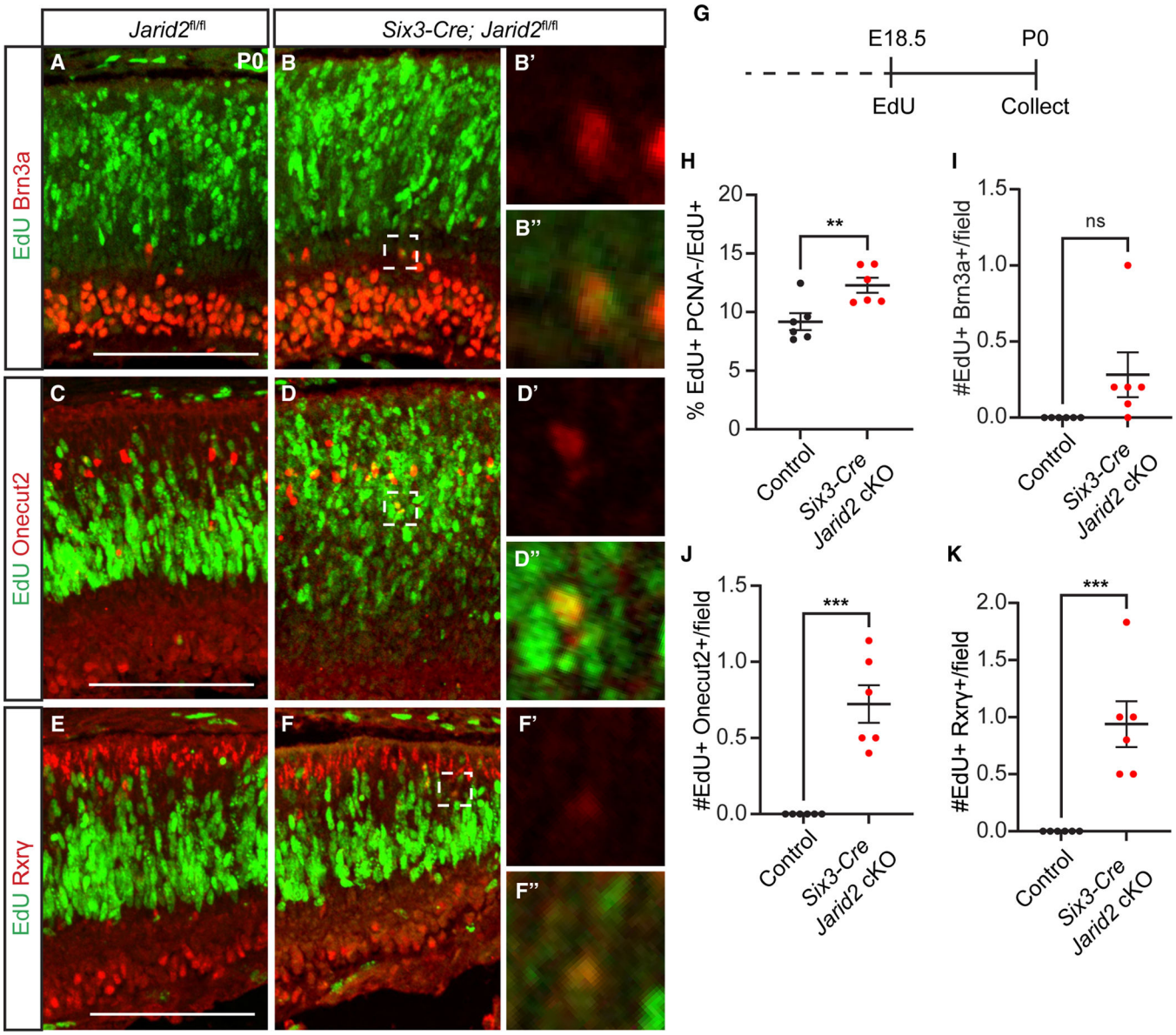

Figure 2. Loss of *Jarid2* promotes extended production of early-born retinal neurons

Animals were administered EdU at E18.5 and analyzed at P0 (G). *Six3-Cre Jarid2* cKO but not control retinas showed EdU-labeled (A, B, and I) Brn3a+ RGCs, (C, D, and J; p = 0.08) Oc2+ horizontal cells, and (E, F, and K) Rxrγ+ cone photoreceptors. (H) Cell-cycle exit (EdU+PCNA−/EdU+) of RPCs was increased in *Six3-Cre Jarid2 cKO* retina. Zoomed-in images were obtained from a single imaging plane. Graphs represent mean ± SEM, n = 6. **p < 0.01, ***p < 0.00 by Student's t test. Scale bars, 100 μm. See also Figure S3 and Table S6 for statistical details.

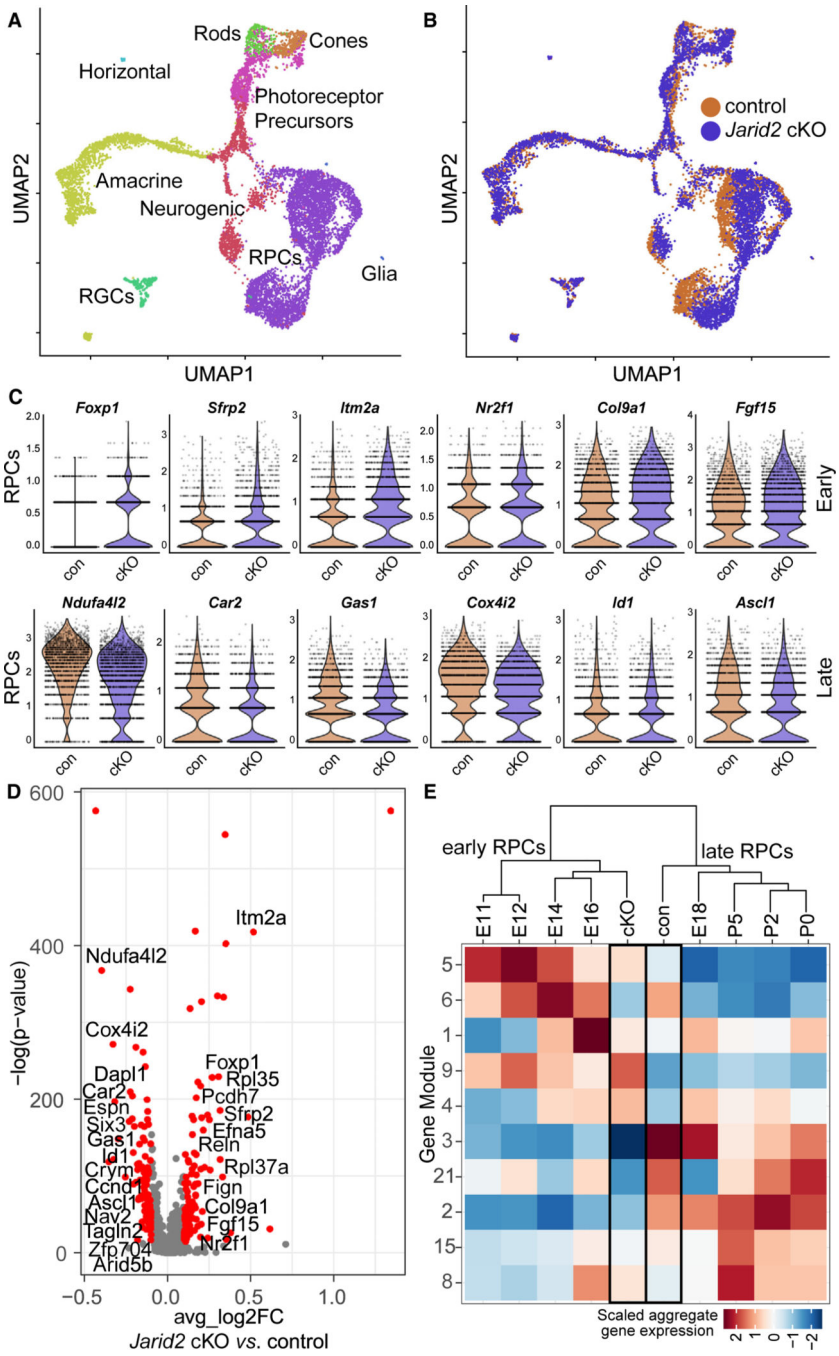

Figure 3. Increased early RPC gene expression in *Rax-Cre Jarid2* cKO RPCs

(A) UMAP dimensional reduction separates single cells from E18.5 retinas into distinct retinal cell types.

(B) Dimensional reduction based on mature transcripts highlights the difference between *Jarid2* cKO and control RPCs.

(C) Violin plots of SCTransform-normalized mature transcript counts in *Jarid2* control and cKO RPCs. These selected early and late RPC genes are significantly differentially

expressed in the two populations by Wilcoxon rank-sum test (default for Seurat FindMarkers function).

(D) Differential expression analysis comparing total gene expression from *Jarid2* cKO and control RPCs. Volcano plot of all expressed genes with significantly changed genes in red. p-adj < 0.05, average log2 fold change > 0.1. Genes are plotted such that those with increased expression in the *Jarid2* cKO are on the right.

(E) Module analysis across retinal RPCs. Heatmap represents scaled aggregate gene expression for RPCs from *Jarid2* cKO, *Jarid2* control, and E11–P5 RPCs (raw data from Clark et al.[11]). See also Figure S4 and Tables S1 and S2.

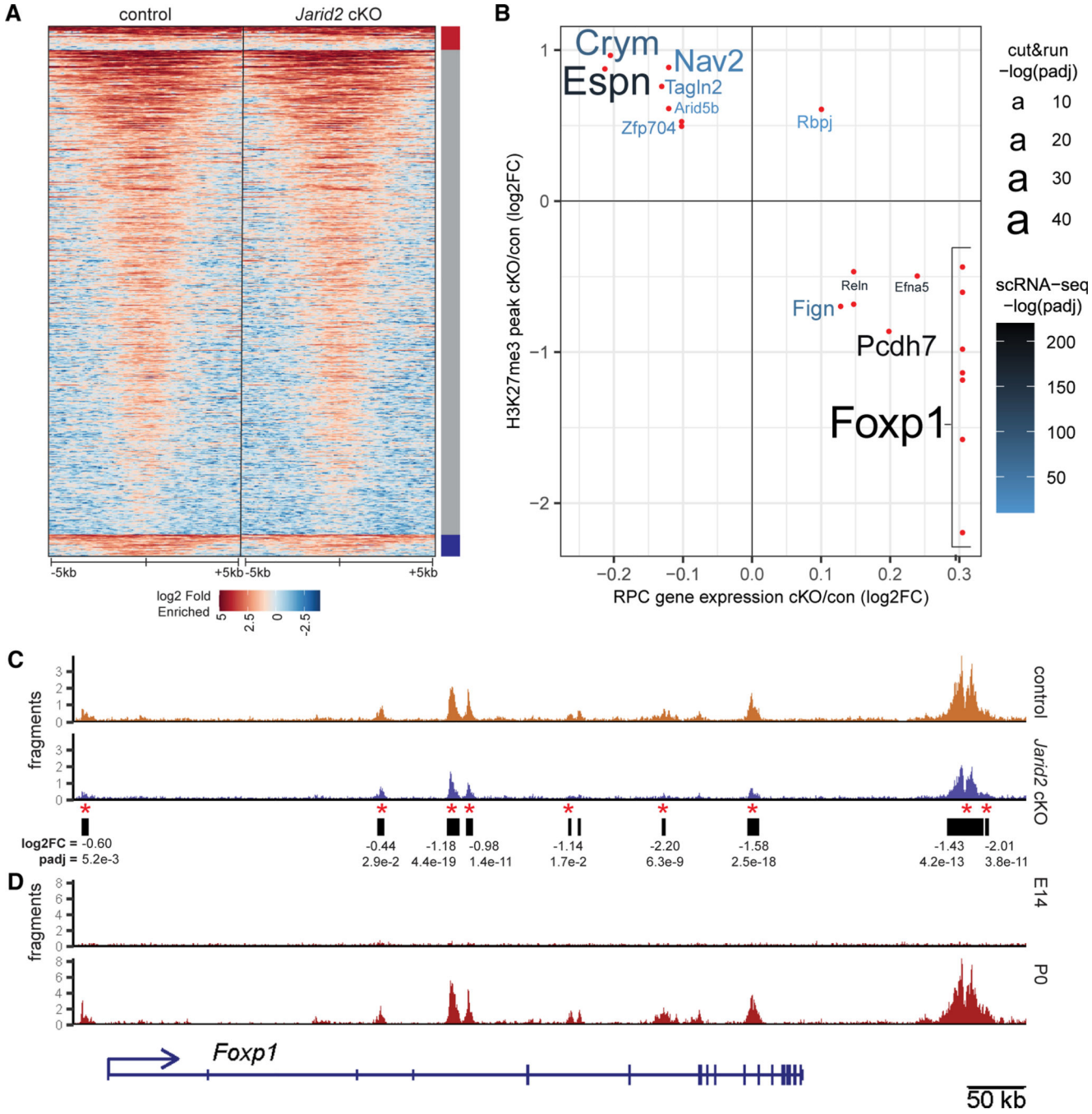

Figure 4. Jarid2 regulates H3K27me3 deposition at select genes

(A) Heatmap of H3K27me3 enrichment compared with IgG, 5 kb to either side of the center of merged peaks called from E18.5 *Jarid2* control and cKO CUT&RUN experiments. Peaks are grouped according to significant increase (red bar), decrease (blue bar), or no change (gray bar) in *Jarid2* cKO. n = 8.

(B) Intersection of gene annotation for differentially regulated H3K27me3 peaks in whole retina and differentially expressed in *Jarid2* cKO RPCs. Those peaks with reduced H3K27me3 and increased associated gene expression in *Jarid2* cKO RPCs are in the bottom

right quadrant. Relative confidence, −log(q value), is indicated by font size for CUT&RUN, or font color for scRNA-seq.

(C) *Jarid2* control and cKO H3K27me3 CUT&RUN reads over the *Foxp1* gene locus and called peaks (black bars). Red asterisk: significantly reduced peaks ($q \leq 0.05$).

(D) H3K27me3 CUT&RUN tracks for wild-type whole retina at E14.5 and P0. See also Figure S6 and Table S3.

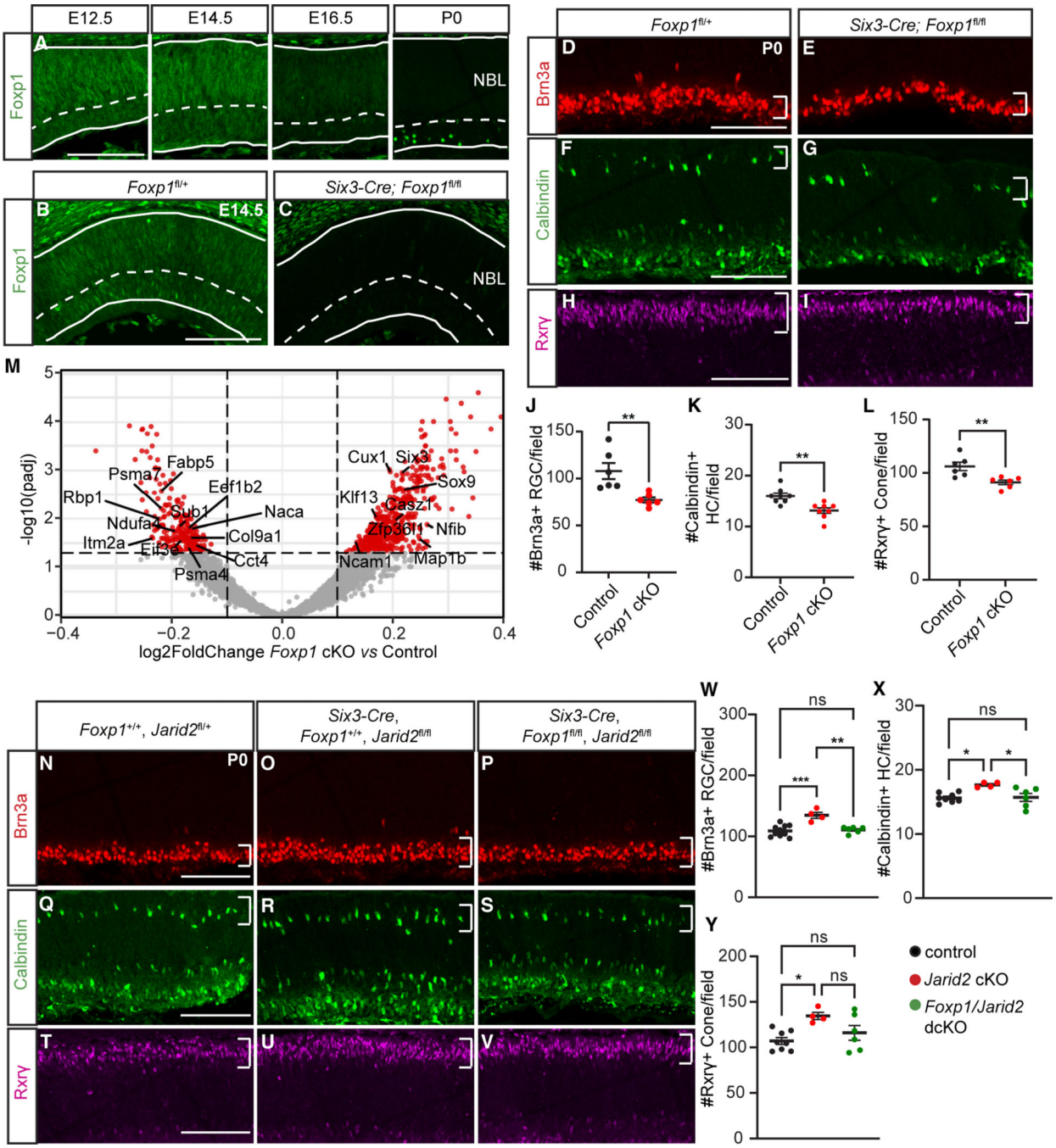

Figure 5. Foxp1 regulates generation of early-born retinal cell types

(A) *Foxp1* expression in wild-type retinas at E12.5, E14.5, E16.5, and P0.

(B and C) Foxp1 expression in the central retina of E14.5 $Foxp1^{fl/+}$ (control) and *Six3-Cre*; $Foxp1^{fl/fl}$ (*Foxp1* cKO) littermates.

(D–L) *Foxp1* cKO retina showed (D, E, and J) reduced Brn3a-labeled RGCs, (F, G, and K) reduced Calbindin-labeled horizontal cells, and (H, I, and L) reduced Rxrγ-labeled cone photoreceptors within central dorsal retinas at P0. Regions of interest marked by white brackets.

(M) Cropped volcano plot of *Foxp1* cKO E16.5 bulk RNA-seq results. Red dots represent significantly differentially expressed genes. p-adj < 0.05.
(N–V) Representative images of early-born retinal cell types in (N, Q, and T), control animals in (O, R, and U), and *Six3-Cre Jarid2* cKO in (P, S, and V), or *Foxp1*:*Jarid2* double cKO littermates at P0 with (W and Y) associated quantification.
(N–P and W) Brn3a-labeled cells, (Q–S and X) Calbindin-labeled horizontal cells, (T–V and Y) Rxrγ-labeled cone photoreceptors. Region of interest marked by white brackets. NBL, neuroblastic layer. Graphs represent mean ± SEM. n = 6 in (J and L) and *Foxp1*:*Jarid2* double cKO in (W–Y), n = 8 in (K), and control in (X and Y), n = 10 in control in (W), n = 4 in *Jarid2* cKO in (W–Y). *p < 0.05, **p < 0.01. ns, not significant. Scale bars, 100 μm. See also Tables S4 and S6 for statistical details.

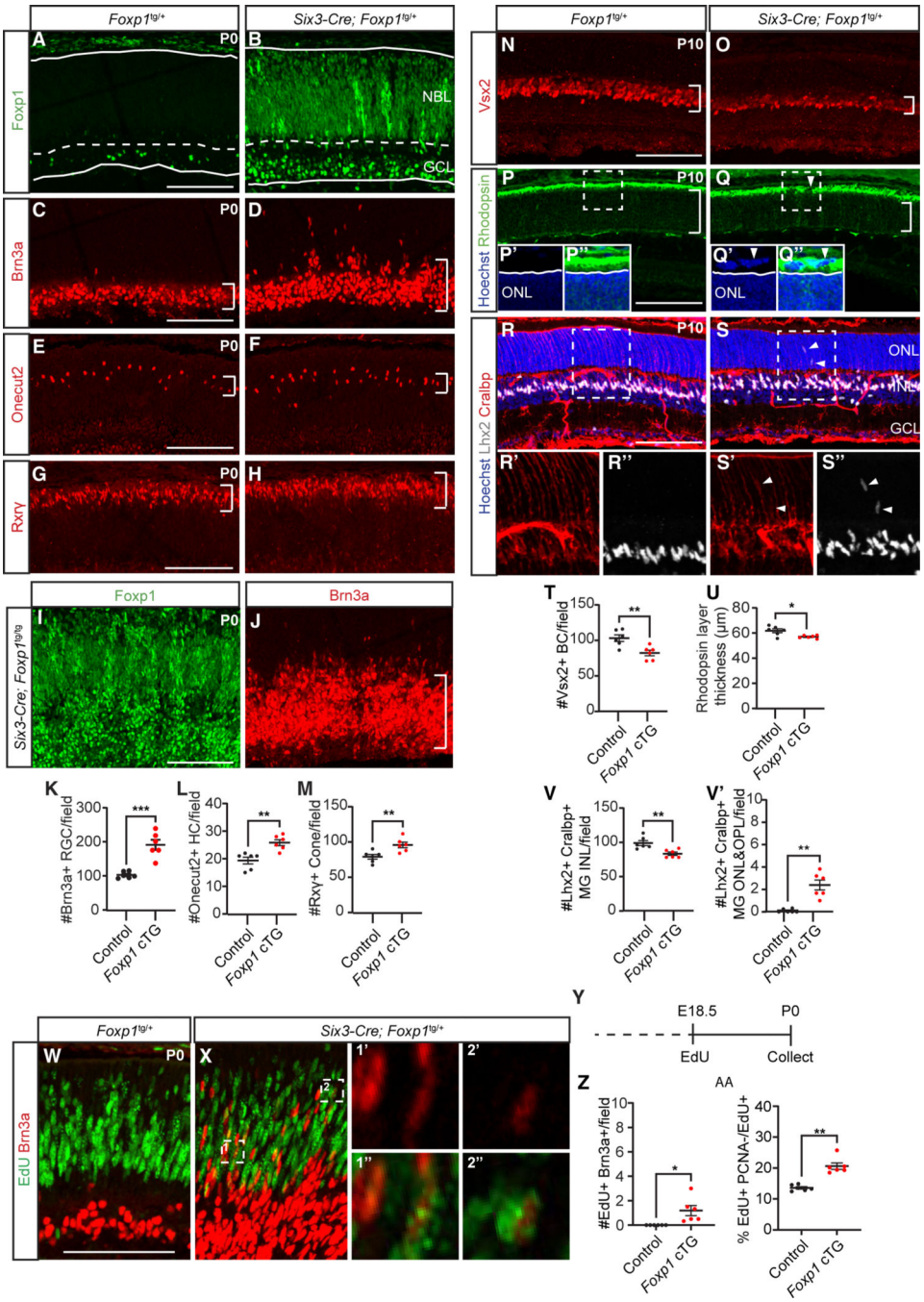

Figure 6. Sustaining *Foxp1* in RPCs increases in early-born and decreases in late-born retinal cells

(A and B) Foxp1 expression in P0 *Foxp1*$^{tg/+}$ (control) and *Six3-Cre*; *Foxp1*$^{tg/+}$ (*Foxp1* cTG) littermates.

(C–H and K–M) *Foxp1* cTG showed increased (C, D, and K) Brn3a-labeled RGCs (E, F, and L) Onecut2-labeled horizontal cells, and (G, H, and M) Rxrγ-labeled cone photoreceptors at P0.

(I and J) Foxp1 expression and Brn3a-labeled RGCs in P0 *Six3-Cre*; *Foxp1*$^{tg/tg}$ retina.

Foxp1 cTG at P10 showed (N, O, and T) decreased Vsx2-labeled bipolar cells and (P, Q, and

U) reduced thickness of Rhodospin-labeled rod photoreceptor layer. Arrowheads in (P) and (Q) indicate abnormal structure in the subretinal region.

(R, S, and V) *Foxp1* cTG had reduced Lhx2 and Cralbp-colabeled Müller glia in the INL and (V′) increased Müller glia in the ONL and OPL. Arrowheads in (S, S', and S′′) indicate mislocated Müller glia in the ONL and OPL.

(Y) *Foxp1* cTG administered EdU at E18.5 and analyzed at P0 (W–Z) showed increased EdU+Brn3a+ RGCs. Zoomed-in images were from a single imaging plane. (AA) *Foxp1* cTG retina showed increased cell-cycle exit of progenitors. NBL, neuroblastic layer; GCL, ganglion cell layer; ONL, outer nuclear layer; INL, inner nuclear layer. Graphs represent mean ± SEM, n = 6. *p < 0.05, **p < 0.01, ***p < 0.001, by Student's t test. Scale bars, 100 μm. See also Figure S7 and Table S6 for statistical details.

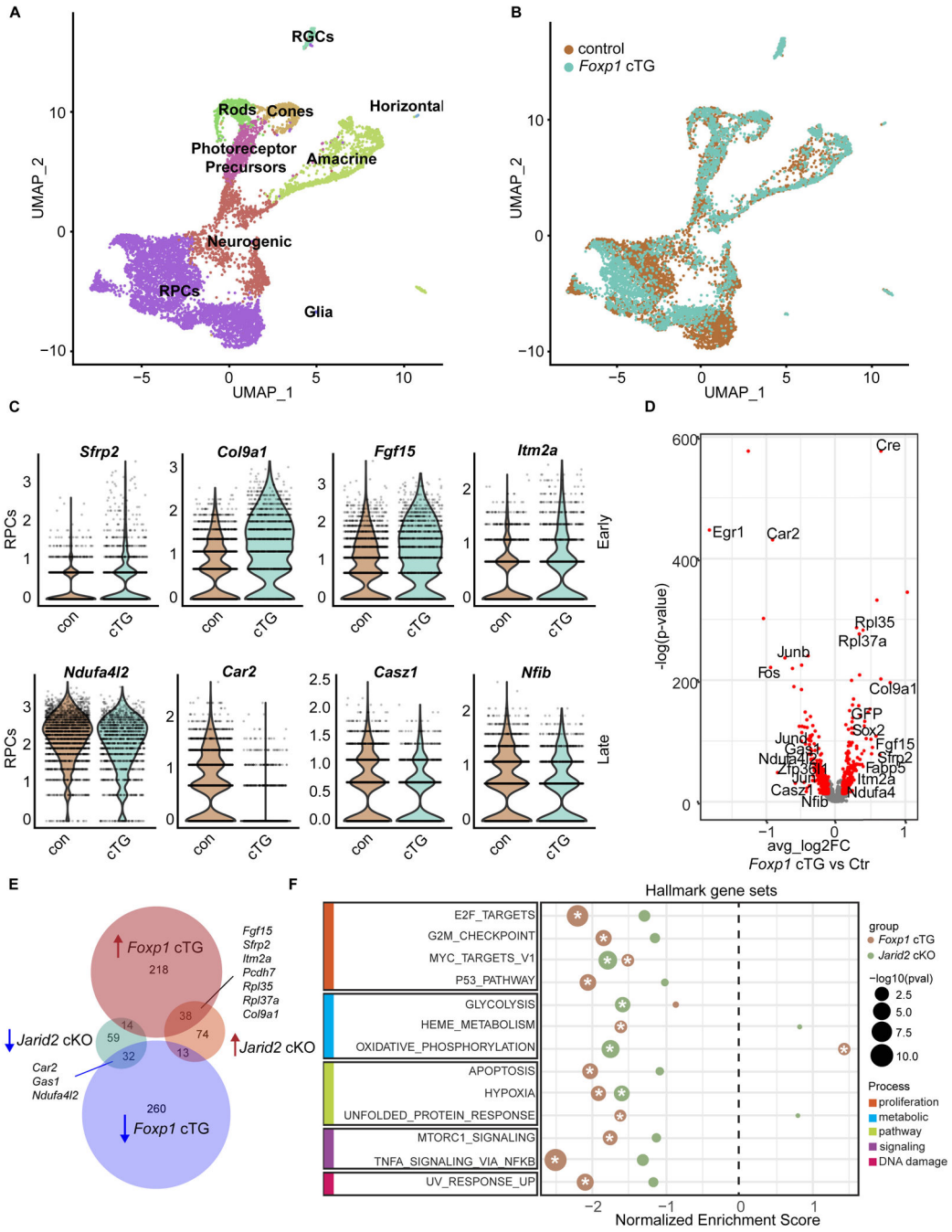

Figure 7. Elevated *Foxp1* expression results in increased early RPC gene expression

(A and B) UMAP dimensional reduction of scRNA-seq data from P0 *Foxp1* cTG and littermate control, colored by annotated cell types (A) and colored by genotype (B).

(C) Violin plots of normalized transcript counts of selected early and late RPC genes differentially expressed in *Foxp1* control and *Foxp1* cTG RPCs.

(D) Volcano plot of all expressed genes, with genes significantly differentially expressed in *Foxp1* cTG in red. p-adj < 0.01, average log2 fold change >0.1. Genes are plotted such that those with increased expression in the *Foxp1* cTG are on the right.

(E) Venn diagram comparing differentially expressed genes common to *Jarid2* cKO and *Foxp1* cTG RPCs. RPC marker genes are shown.

(F) GSEA of MSigDB mouse hallmark gene sets. A positive enrichment score indicates enrichment in *Jarid2* cKO (green) and *Foxp1* cTG (brown) RPCs, while a negative score represents enrichment in the control. Significantly enriched genes sets (p-adj < 0.05) are marked with an asterisk. Gene sets are grouped by shared biological process. See also Table S5.

KEY RESOURCES TABLE

REAGENT or RESOURCE	SOURCE	IDENTIFIER
Antibodies		
Goat anti-Brn3 (1:50)	Santa Cruz Biotechnology	Cat#sc6026; RRID: AB_673441
Mouse anti-Brn3a (1:200)	Millipore	Cat#MAB1585; RRID: AB_94166
Mouse anti-Otx2 (1:200)	Santa Cruz Biotechnology	Cat#sc-514195
Rabbit anti-calbindin D-28K (1:2000)	Millipore	Cat#PC253L; RRID: AB_213554
Mouse anti-Rxrγ (1:250)	Santa Cruz Biotechnology	Cat#sc-365252; RRID: AB_10850062
Rabbit anti-recoverin (1:2000)	Millipore	Cat#AB5585; RRID: AB_2253622
Goat anti-Vsx2/Chx10 (1:500)	gift from Dr. Edward M. Levine	N/A
Sheep anti-Vsx2/Chx10 (1:500)	Exalpha Biologicals	Cat#X1180P; RRID: AB_2314191
Mouse anti-Rhodopsin (1:200)	Thermo Fisher Scientific	Cat#MA5–11741; RRID: AB_10980983
Rabbit anti-Lhx2 (1:500)	Abcam	Cat# ab184337, RRID: AB_2916270
Mouse anti-Cralbp (1:500)	Novus	Cat# NB100–74392, RRID: AB_2253681
Mouse anti AP-2alpha (1:500)	Santa Cruz Biotechnology	Cat#sc-12726, RRID: AB_667767
Mouse anti-PCNA (1:2000)	Sigma-Aldrich	Cat#P8825, RRID: AB_477413
Rabbit anti-pH3 (Ser10) (1:250)	Millipore	Cat#06–570; RRID: AB_310177
Rabbit anti-Foxp1 (1:2000)	Abcam	Cat#ab16645; RRID: AB_732428
Rabbit anti-H3K27me3	Millipore	Cat#07–449; RRID: AB_310624
Sheep anti-Onecut2 (1:100)	R&D Systems	Cat#AF6294; RRID: AB_10640365
Donkey anti-rabbit 488 (1:400)	Thermo Fisher Scientific	Cat#A-21206, RRID: AB_2535792
Donkey anti-rabbit 555 (1:400)	Thermo Fisher Scientific	Cat#A31572; RRID: AB_162543
Donkey anti-mouse 488 (1:400)	Thermo Fisher Scientific	Cat#A-21202, RRID: AB_141607
Donkey anti-mouse 555 (1:400)	Thermo Fisher Scientific	Cat#A-31570, RRID: AB_2536180
Donkey anti-sheep 555 (1:400)	Thermo Fisher Scientific	Cat#A-21436, RRID: AB_2535857
Donkey anti-goat 488 (1:400)	Thermo Fisher Scientific	Cat#A-11055, RRID: AB_2534102
Chemicals, peptides, and recombinant proteins		
DNAse I	Sigma-Aldrich	Cat#D4513
Liberase	Sigma-Aldrich	Cat#5401119001

REAGENT or RESOURCE	SOURCE	IDENTIFIER
RBC lysis buffer	eBioscience	Cat#00–4333-57
Tamoxifen	Sigma-Aldrich	Cat#T5648
Critical commercial assays		
Click-iT plus EdU Imaging Kits	Thermo Fisher Scientific	Cat#C10637
RNeasy Plus Mini Kit	Qiagen	Cat#74134
CUT&RUN Assay Kit	Cell Signaling	Cat#86652
Spin column Kit for Cut&Run	Cell Signaling	Cat#14209
RNA ScreenTape Assay	Agilent Technologies	Cat#5067–5576, 5067–5577, 5067–5578
D1000 ScreenTape Assay	Agilent Technologies	Cat#5067–5582, 5067–5583
Kapa Library Quant Kit	Kapa Biosystems	Cat#KK4824
NEBNext Ultra II Directional RNA Library Prep Kit for Illumina	New England Biolabs	Cat#E7760
NEBNext rRNA Depletion Kit v2	New England Biolabs	Cat#E7400
NEBNext UItra II DNA Library Prep Kit for Illumina	New England Biolabs	Cat#E7645
Chromium Single Cell 3′ Library Prep Kit v3	10X Genomics	Cat#PN-1000092
Chromium Next GEM Single Cell 3′ Library Prep Kit v3.1	10X Genomics	Cat#PN-1000128
NovaSeq XP workflow v1 and v1.5	Illumina	Cat#20021664, 20043131
NovaSeq S2 and S4 Reagent Kits	Illumina	Cat#20012860, 20028312
Deposited data		
All raw and analyzed data generated for this study	This paper	GEO: GSE202741
Jarid2 cKO scRNA-seq	This paper	GEO: GSE202734
H3K27me3 CUT&RUN from Jarid2 cKO	This paper	GEO: GSE222955
H3K27me3 CUT&RUN from E14.5 and P0 retina	This paper	GEO: GSE202728
Foxp1 cKO RNA-seq	This paper	GEO: GSE202725
Foxp1 cTG scRNA-seq	This paper	GEO: GSE222956
Single Cell-seq of whole retina E11.5 to P5	Clark et al.[11]	GEO: GSE118614
H3K27me3 ChIP-seq from E17.5, P0, and P3 retina	Aldiri et al.[29]	GEO: GSE87037
Experimental models: Organisms/strains		

REAGENT or RESOURCE	SOURCE	IDENTIFIER
C57BL/6N-Jarid2$^{tm1a(KOMP)Wtsi}$/Mmucd mice	KOMP Repository	RRID: MMRRC_048262-UCD
B6.Cg-Tg(ACTFLPe)9205Dym/J mice	Jackson Laboratory	RRID: IMSR_JAX:005703
Tg(Six3-Cre)69Frty mice	Dr. Yasuhide Furuta (Furuta et al.[52])	RRID: IMSR_JAX:019755
Rax$^{tm1.1(cre/ERT2)Sbls}$/J mice	Dr. Seth Blackshaw (Pak et al.[53])	RRID: IMSR_JAX:025521
Foxp1$^{flox/flox}$ mice	Jackson Laboratory (Feng et al.[60])	RRID: IMSR_JAX:017699
Foxp1a transgenic mice	Dr. Hui Hu (Wang et al.[61])	MGI:5607369
Software and algorithms		
BBTools v38.34	Bushnell et al.[70]	RRID:SCR_016968
cutadapt v1.16 and v2.8	Martin[71]	RRID:SCR_011841
STAR v2.7.0f and v2.7.6a	Dobin et al.[72]	RRID:SCR_004463
featureCounts v1.5.1	Liao et al.[73]	RRID:SCR_012919
DESeq2 v1.38.1	Love et al.[74]	RRID:SCR_015687
CellRanger v3.1.0	10X Genomics	RRID:SCR_023221
velocyto v0.17.17	La Manno et al.[75]	RRID:SCR_018167
Seurat v4.0.3	Stuart et al.[87]	RRID:SCR_007322
DoubletFinder v2.0.3	McGinnis et al.[76]	RRID:SCR_018771
Monocle3 v1.0.0	Qiu et al.[55]	RRID:SCR_018685
Novoalign v4.02.02	Novocraft	RRID:SCR_014818
Samtools v1.10	Danecek et al.[77]	RRID:SCR_002105
Macs2 v2.2.7.1	Zhang et al.[78]	RRID:SCR_013291
Fgsea v1.18.0	Korotkevich et al.[79]	RRID:SCR_020938
Gage v2.42.0	Luo et al.[80]	RRID:SCR_017067
GraphPad Prism v9	GraphPad	RRID:SCR_002798
NIS-Elements v18	Nikon	RRID:SCR_014329